Distinct stem-like cell populations facilitate functional regeneration of the *Cladonema* medusa tentacle

[1] Sosuke Fujita, [1] Erina Kuranaga, [2] Masayuki Miura, and [2] Yu-ichiro Nakajima*

1. Graduate School of Life Sciences, Tohoku University
2. Graduate School of Pharmaceutical Sciences, The University of Tokyo

*Author for correspondence e-mail: nakaji97@g.ecc.u-tokyo.ac.jp
Tel: +81-3-5841-4863

Running title: Distinct stem-like cells enable tentacle regeneration in jellyfish
Main text: 6352 words (Abstract: 186 words)
Figures: 6 **Supplementary information** (Figures: 8)
Keywords: regeneration, blastema, non-bilaterians, cnidarians, jellyfish, tentacle, i-cell

Abstract

Blastema formation is a crucial process that provides a cellular source for regenerating tissues and organs. While bilaterians have diversified blastema formation methods, its mechanisms in non-bilaterians remain poorly understood. Cnidarian jellyfish, or medusae, represent early-branching metazoans that exhibit complex morphology and possess defined appendage structures highlighted by tentacles with stinging cells (nematocytes). Here we investigate the mechanisms of tentacle regeneration, using the hydrozoan jellyfish *Cladonema pacificum*. We show that proliferative cells accumulate at the tentacle amputation site and form a blastema composed of cells with stem-like cell morphology. Lineage tracing experiments indicate that repair-specific proliferative cells in the blastema are distinct from resident stem-like cells. We further demonstrate that resident stem-like cells control nematogenesis and tentacle elongation during both homeostasis and regeneration, while repair-specific proliferative cells preferentially differentiate into epithelial cells in the newly formed tentacle, analogous to lineage-restricted stem/progenitor cells observed in salamander limbs. Taken together, our findings reveal a regeneration mechanism that utilizes both resident stem-like cells and repair-specific proliferative cells, which in conjunction efficiently enable functional appendage regeneration, and provide novel insight into the diversification of blastema formation across animal evolution.

Introduction

Regeneration, the phenomenon of re-forming missing body parts, is widespread among metazoans. Common regeneration processes include wound closure immediately after injury; formation of the cellular source, or blastema, that reconstitutes the lost tissue; and regrowth of the tissue that integrates different cellular behaviors such as proliferation and differentiation (McCusker et al., 2015). Among these regenerative responses, blastema formation is a critical step that can distinguish regenerative and non-regenerative systems. Indeed, most mammalian and avian species do not form blastema upon injury while wound closure normally occurs (Seifert and Muneoka, 2018). Understanding blastema formation mechanisms in highly regenerative animals may thus help us identify the necessary elements to potentially improve our regenerative abilities.

Blastema is defined as undifferentiated cells with mitotic capacity that appear after damage such as amputation or irradiation (Aztekin, 2021; Bely and Nyberg, 2010). Accumulating evidence has suggested that methods of blastema formation vary among animals with high regenerative abilities (Tanaka and Reddien, 2011). For example, in planarians, pluripotent stem cells called neoblasts that are distributed throughout the body, are recruited to the injury site to produce blastema (Reddien and Alvarado, 2004). Salamanders can regenerate adult limbs upon amputation via blastema formation, but the underlying cellular mechanisms vary among species: in the axolotl, tissue-specific stem cells contribute to blastema, while in the newt, muscle fibers dedifferentiate into proliferative progenitor cells to behave as blastema (Sandoval-Guzmán et al., 2014). During zebrafish caudal fin regeneration, both osteoblast-derived dedifferentiated cells and resident progenitor cells migrate to the wound site to form blastema (Ando et al., 2017; Knopf et al., 2011). These studies support the idea that the supply of blastema has diversified across the animal kingdom, whose members utilize resident stem/progenitor cells and/or repair-specific *de novo* proliferative cells to reconstruct lost body parts. While mechanisms of blastema formation have been intensively studied in the limited number of regenerative animals, little is known about their evolutionary characteristics: which elements are acquired as lineage-specific novelties and which are widely conserved within highly regenerative species? In particular, the current

91 understanding of blastema formation largely relies on bilaterian models, and thus the
92 mechanisms of blastema formation outside of bilaterians remain poorly understood.
93 Among various regeneration contexts, appendage regeneration is widely
94 observed in bilaterians (e.g. amphibian limbs and fish fins), and is suitable for
95 understanding the evolution of regenerative processes (Aztekin, 2021; Daponte et al.,
96 2021). The bilaterian program of blastema formation during appendage regeneration is
97 associated with repair-specific stem/progenitor cells (Knopf et al., 2011; Lehoczky et al.,
98 2011; Sandoval-Guzmán et al., 2014). Yet, to elucidate the evolutionary history of
99 blastema formation programs, their mechanisms must be studied in early-branching
100 metazoans in addition to bilaterian models.
101 Cnidarians (corals, sea anemones, hydroids, and jellyfish) are among the earliest
102 branching metazoans, composed of two major groups Anthozoa and Medusozoa,
103 forming a diverse phylum that contains over 10,000 species, and stand at a unique
104 phylogenetic position as the sister group to bilaterians (Figure 1A). While cnidarians
105 display considerably divergent morphologies and life cycles, represented by the polyp
106 and medusa stages; their common traits are a diploblastic radially-symmetric body
107 along with tentacles as the well-defined appendages that bear the stinging cells,
108 nematocytes (cnidocytes) (Fritz et al., 2013; Technau and Steele, 2011). Although
109 regenerative potential may vary among the group, most documented cnidarian species
110 are capable of regenerating lost tissues and organs, and some can even regenerate
111 their entire body (Fujita et al., 2021; Holstein et al., 2003).
112 Among cnidarians, polyp-type animals such as *Hydra*, *Hydractinia,* and
113 *Nematostella* have been utilized as models to understand the mechanism of whole-body
114 regeneration; including patterning, body axis formation, and mechanical responses
115 (Gahan et al., 2016; Röttinger, 2021; Vogg et al., 2019). After mid-gastric bisection in
116 *Hydra*, cell proliferation of the stem cells, or i-cells, around the wound site is accelerated
117 by Wnt3a produced from dying cells to generate blastema (Chera et al., 2009). Upon
118 decapitation of the colony polyp *Hydractinia*, i-cells remotely located in the body column
119 migrate to the injury site to form blastema (Bradshaw et al., 2015). During head
120 regeneration of the sea anemone *Nematostella*, two adult stem-like cell populations,
121 fast-cycling cells in the body wall epithelium and slow-cycling cells in the mesenteries,
122 migrate toward the amputation site to form blastema (Amiel et al., 2019). These studies

suggest that the recruitment of resident stem cells to the injury site is prerequisite for blastema formation after amputation of the body. However, it remains unclear whether repair-specific proliferative cells constitute the cellular source of blastema during cnidarian regeneration.

In contrast to the sessile polyp stage, medusae, commonly called jellyfish, exhibit a more complex body structure that includes multiple types of muscle such as smooth and striated muscles, developed neural networks, and distinct organs and appendages, which together enable free swimming and avoidance behaviors (Katsuki and Greenspan, 2013; Leclère and Röttinger, 2017). While most sexually-reproducing medusae do not clonally propagate like polyps, medusae can still regenerate various organs and appendages (e.g., manubrium, tentacle, umbrella, gonad, eye) after injury and reconstitute *de novo* structures after their removal (Fujita et al., 2019; Gamero-Mora et al., 2019; Ostendarp et al., 2022; Sinigaglia et al., 2020; Stamatis et al., 2018; Stierwald et al., 2004; Weber, 1981). A recent report using the hydrozoan jellyfish *Clytia* has suggested that, upon removal of the entire manubrium, i-cells and differentiated cells localized in neighboring organs migrate to the damage site through the canals, contributing to *de novo* manubrium regeneration (Sinigaglia et al., 2020). Despite the importance of proliferating blastema cells in highly regenerative animals, the detailed mechanisms of organ and appendage regeneration in medusae, particularly the mechanism of blastema formation and its specific role are largely unknown.

The hydrozoan jellyfish *Cladonema pacificum* is an emerging jellyfish model that has been utilized to study development and physiology (Fujiki, 2019; Masuda-Ozawa et al., 2022; Takeda et al., 2018). Because *Cladonema* allows for easy lab maintenance with its high spawning rate, it enables monitoring all life cycle stages and exploring organismal responses to different stimuli. The genus *Cladonema* is morphologically characterized by branched tentacles at the medusa stage (Figure 1B) (Fujiki, 2019; Rees, 1979; Suga et al., 2008; Zhou et al., 2022). The *Cladonema* medusa tentacle is primarily composed of bi-layered epithelial tissues (ectoderm and endoderm): i-cells, neurons, and nematocytes are located in the ectodermal layer while neurons and gland cells are located in the endodermal layer. Resident stem-like cells, i-cells, are localized at the basal side of the tentacle (tentacle bulb), and are thought to give rise to progenitors and differentiated cells during normal development and homeostasis

155 (Denker et al., 2008; Fujita et al., 2019). The continuous growth and branching potential
156 of the medusa tentacle makes it an attractive model to understand the mechanisms of
157 appendage morphogenesis, growth, and regeneration in cnidarians.
158 In this study, we investigate the cellular mechanism of appendage regeneration
159 using the *Cladonema* medusa tentacle. Establishing the *Cladonema* tentacle as an
160 organ that can efficiently and functionally regenerate upon amputation, we show that
161 highly proliferative cells accumulate at the injury site within 24 hours to behave as
162 blastema. Lineage tracing experiments using nucleoside analogs as well as dye labeling
163 reveal that blastema cells are not derived from resident i-cells but rather appear locally
164 after damage. We further identify the role of blastema cells as the principal cellular
165 source of the epithelium in the newly formed tentacle, while resident i-cells contribute to
166 nematogenesis and tissue elongation during both homeostasis and regeneration. These
167 results suggest the existence of two distinct proliferative cell populations: blastema as
168 repair-specific proliferative cells and resident i-cells as homeostatic proliferative cells,
169 both of which collectively enable functional tentacle regeneration. In a broader context,
170 our findings highlight the diversification of blastema formation in non-bilaterian systems,
171 providing an evolutionary insight into animal regeneration.
172
173
174 ## Materials and Methods
175
176 **Animal cultures and surgical manipulations**
177 *Cladonema pacificum* (female strain 6W) medusae were used for this research. The
178 medusae were maintained in plastic containers (V-type container, V-7, V-8, and V-9; AS
179 ONE) at 22 ℃ in artificial sea water (ASW). ASW was prepared using SEA LIFE (Marin
180 Tech) dissolved in tap water with chlorine neutralizer (Coroline off; GEX Co. ltd) (24
181 p.p.t). The medusae were fed Vietnamese brine shrimp (A&A Marine LLC).
182 Before surgical manipulation, the medusae were anesthetized with 7% $MgCl_2$ in
183 deionized water for 2 min in a petri dish (Falcon, #351008). Surgical manipulations were
184 performed with micro scissors (Teraoka, NY33408). After manipulations, the medusae
185 were quickly returned to ASW. When the tentacle was amputated with the bulb left
186 intact, the medusae were fed 1 day before manipulation and were starved after

187 amputation. When the tentacle was amputated along with the bulb, the medusae were
188 fed 1 day before manipulation and were fed 3 times a week afterward.
189 Bright field pictures of medusae were taken with a LEICA S8APO microscope
190 with a Nikon digital camera (D5600).
191
192 **Immunofluorescence**
193 The medusae were anesthetized with 7% $MgCl_2$ in deionized water for 5 min
194 and fixed at room temperature (R.T.) for 1 h or overnight at 4 ℃ with 4%
195 paraformaldehyde (PFA) in ASW. After fixation, the samples were washed three times
196 (10 min each) with PBS containing 0.1% Triton X-100 (0.1% PBT). The samples were
197 incubated in primary antibodies in 0.1% PBT overnight at 4 ℃. The antibodies used
198 were rabbit anti-Phospho-Histone H3 (Ser10) (1:500; Upstate, 06–570), mouse anti-β-
199 catenin (8E4) (1:100; Sigma-Aldrich, ALX-804-260-C100), and mouse anti-PKC ζ C20
200 (1:100; Santa Cruz, sc-216). After primary antibody incubation, the samples were
201 washed three times (10 min each) with 0.1% PBT. The samples were incubated with
202 secondary antibodies (1:500; ALEXA FLUOR 488, 555, 647 Goat anti-mouse IgG,
203 ALEXA FLUOR 488, 555, 647 Goat anti-rabbit IgG; Thermo Fisher Scientific, A28175,
204 A-11008) and Hoechst 33342 (1:500; Thermo Fisher Scientific, H1399) in 0.1% PBT for
205 1 h in the dark. After three washes (10 min each) in 0.1% PBT, the samples were
206 mounted on slides with 70% glycerol. Nuclear and poly-γ-glutamate were stained with
207 DAPI (1:250; Invitrogen, D1306), and actin fibers were stained with Alexa 546 phalloidin
208 (1:400; Invitrogen, A22283) in 0.1% PBT for 1 h. Confocal images were collected
209 through a Zeiss LSM 880 confocal microscope. Image processing (color display) and
210 quantification were performed using ImageJ/Fiji software.
211
212 **EdU labeling**
213 The medusae were incubated with 20 or 150 μM 5-ethynyl-2'-deoxyuridine (EdU) (EdU
214 kit; Invitrogen, C10337) in ASW for 1h or 24 h. In chase labeling, the medusae were
215 washed with ASW at least twice (up to three times, depending on amount). In pulse
216 labeling, after EdU treatment, the medusae were anesthetized with 7% $MgCl_2$ in
217 deionized water and fixed 4% PFA in ASW. After fixation, the samples were washed
218 and incubated with a EdU reaction cocktail (1× reaction buffer, $CuSO_4$, Alexa Fluor

219 azide 488 or 647, and 1× reaction buffer additive; all included in EdU kit; Invitrogen,
220 C10337 or C10340) for 30 min in the dark. After the EdU reaction, the samples were
221 washed and incubated with Hoechst 33342 in 0.1% PBT for 30 min.
222 In combination with antibody staining, EdU reaction was performed after
223 incubation with the secondary antibody. To combine EdU labeling with fluorescent *in*
224 *situ* hybridization (FISH), the EdU reaction was performed after the incubation with Cy5-
225 tyramide solution. In combination with DAPI poly-γ-glutamate staining, the EdU reaction
226 was performed before incubation with DAPI.
227
228 **EdU and BrdU dual labeling**
229 The medusae were incubated with 150 μM EdU in ASW for 1h or 24 h before
230 amputation, depending on the experiments. Just after incorporation of EdU, the
231 medusae were washed in ASW three times, and tentacles were amputated. At 24 hpa,
232 the medusae were incubated with 2.5 mM BrdU in ASW for 1h. The medusae were
233 washed out in ASW three times.
234 The medusae were anesthetized with 7% $MgCl_2$ for 5 min and fixed with 4%
235 PFA in ASW. The samples were washed three times with 0.1% PBT and incubated with
236 a EdU reaction cocktail for 30min in dark. The samples were washed three times and
237 treated with 2N HCl for 30min and then washed three times and incubated in primary
238 antibodies in 0.1% PBT overnight at 4 ℃. The primary antibody used was mouse anti-
239 BrdU (1:100; BD, #347580). The samples were washed three times and incubated with
240 secondary antibodies (1:500; ALEXA FLUOR 555 Goat anti-mouse IgG) and Hoechst
241 33342 in 0.1% PBT for 1 h in the dark and washed three times.
242
243 **Fluorescent *in situ* hybridization**
244 The following FISH protocol was created from the published protocol (Fujita et al.,
245 2022). The sequence of *Nanos1* and *Piwi* was previously described (Hou et al., 2021),
246 the presumptive sequence of *Minicollagen1* (*Mcol1*) was acquired from Dr. Kumano,
247 and *Nematocyte Outer Wall Antigen* (*Nowa*) was acquired from the annotation of our
248 RNA-seq results. Purified total RNA was reverse transcribed into cDNA by PrimeScript
249 II 1st strand cDNA Synthesis Kit (Takara, 6210A). The target gene fragments were
250 amplified from a cDNA library. The primer sets used for PCR cloning are as follows:

251 *Mcol1*: 5′-CTCGTCGGTATTGCCCTCTC-3′ (forward) and 5′-
252 CCAACCTATCGTGGACGTGT-3′ (reverse), *Nowa*: 5′-GGTCGGTCGAAAGCCACTAA-
253 3′ (forward) and 5′-CCAGGAGGTGAAAGCGAGTT-3′ (reverse). PCR products were
254 sub-cloned into the TAK101 vector (TOYOBO). The resulting plasmids were used for
255 RNA probe synthesis with digoxigenin (DIG) labeling mix (Roche, #11277073910), and
256 T7 (Roche, #10881767001) or T3 RNA polymerase (Roche, #11031163001) was used,
257 according to the insert direction.
258 Medusae were anesthetized 7% $MgCl_2$ for 5 min and fixed overnight at 4 ℃ with
259 4% PFA in ASW. Briefly, fixed samples were washed three times with PBS containing
260 0.1% Tween-20 (PBST), followed by pre-hybridization in hybridization buffer (HB buffer:
261 5 × SSC, 50% formamide, 0.1% Tween-20, 50 μg/ml tRNA, 50 μg/ml heparin) at 55 ℃
262 for 2 h. The samples were hybridized with HB Buffer containing the antisense probes
263 (final probe concentration: 0.5–1 ng/μL in HB Buffer) at 55 ℃ overnight. The samples
264 were washed twice each with wash buffer 1 (5 × SSC, 50% formamide, 0.1% Tween-
265 20), wash buffer 2 (2 × SSC, 50% formamide, 0.1% Tween-20), and 2 × SSC. The
266 samples were then washed with 0.1% PBST and incubated in 1% blocking buffer (1%
267 blocking reagent [Roche] in Maleic acid) for 1 h. The samples were incubated with anti-
268 DIG-POD antibodies (1:500; Roche, #11207733910) in 1% blocking buffer overnight at
269 4 ℃. The samples were then washed with Tris-NaCl-Tween Buffer and incubated with
270 Cy5-tyramide solution (TSA Plus Cyanine 5; AKOYA Biosciences, NEL745001KT) for
271 10 min. Finally, the samples were washed with 0.1% PBST and incubated with Hoechst
272 33342 in 0.1% PBST for 30 min in the dark and washed three times.
273
274 **DiI injection**
275 Medusae were relaxed in 7% $MgCl_2$ on a petri dish. 10 mM CellTracker CM-DiI
276 (Invitrogen, C7001) was injected into the ectodermal layer of the tentacle bulb, using a
277 micro injector (Eppendorf, Femtojet 4i). The quartz capillary (Sutter Instrument, QF100-
278 70-10) was pulled by Laser-Based Micropipette Puller P2000 (Sutter Instrument). After
279 injection, injected tentacles were amputated. At 24 hpa, the injected medusae were
280 incubated with 150 μM EdU in ASW for 1h. The medusae were relaxed in 7% $MgCl_2$ and
281 fixed in 4% PFA. After washing in 0.1% PBT, the medusae were incubated with an EdU

282 reaction cocktail for 30 min in the dark. After the EdU reaction, the samples were
283 washed and incubated with Hoechst 33342 in 0.1% PBT.
284
285 **X-ray irradiation**
286 The medusae were placed in a V7 plastic container with 6-8 ml of ASW, the minimum
287 required for their maintenance. X-ray irradiations were performed using an X-ray
288 machine (mediXtec, MX-160Labo). Medusae were positioned 19 cm from the X-ray
289 source, and a dose of 30 Gy (19.3 minutes at 160 kV 3 mA) was delivered. After
290 irradiation, the medusae were moved to a plastic container with fresh ASW.
291
292 **qPCR**
293 Total RNA was purified from the whole bodies of three medusae with RNeasy Mini kits
294 (Qiagen). Lysate was treated with DNase I (Qiagen, #79254) for 15 min at RT. cDNA
295 was synthesized from 200 ng of total RNA by Prime script RT master Mix (Takara,
296 RR036A). RT-qPCR was performed using TB Green Premix Ex TaqII (Tli RNaseH Plus)
297 (Takara, RR820L) and a Quantstudio6 Flex Real-Time PCR system (Thermo Fisher)
298 using *F-actin capping protein subunit beta* as an internal control (Masuda-Ozawa et al.,
299 2022). The qPCR primer sets are as follows: *CpCapZbeta*: 5'-
300 AAAGAAAGCTGGAGACGGTTCA-3' (Forward), 5'-GTAGTGGGCATTTCTTCCGC-3'
301 (Reverse), *Nanos1*: 5'-TTCGTCAAGTGGCAGTCGTG-3' (Forward), 5-
302 CAAGCCCTGGTACAAACGGA-3' (Reverse).
303
304 **UV laser exposure**
305 Tentacles were amputated at 1 day before UV exposure. At 24 hpa, the medusae were
306 incubated with Hoechst 33342 (1:250) for 20 min and washed three times in ASW. After
307 washing, the relaxed medusae were placed on slides with 7% $MgCl_2$ and enclosed with
308 cover glass. UV laser was exposed to the blastema region of the amputated tentacle
309 using the photo bleaching application (50 cycles at 100% 405 laser power) of the Zeiss
310 LSM 880 confocal microscope. The bleached region is shown with a white dot square
311 (400 x 400 pixels, W x H) in Figure S8B. After UV exposure, the medusae were moved
312 to ASW in plastic containers and monitored to examine the effect on regeneration.
313

Results

For cnidarians, tentacles are essential and common appendages for capturing prey and defending against predators. Cnidarian polyps such as *Hydra*, *Hydractinia*, and *Nematostella* have tentacles in the head region, near the hypostome, which can restore functional tentacles during head regeneration (Bradshaw et al., 2015; Passamaneck and Martindale, 2012; Vogg et al., 2019). Similarly, studies using hydrozoan jellyfish have shown that medusae tentacles can regenerate upon amputation (Fujita et al., 2019; Sinigaglia et al., 2020). Although cnidarians commonly exhibit high regenerative capacity for tentacles, the exact cellular processes and the limitation of regeneration are poorly understood.

To monitor the process of tentacle regeneration and to explore its responses to different dissections, we utilized the medusa tentacle of the hydrozoan jellyfish *Cladonema* (Figure 1). In *Cladonema* tentacles, proliferative cells including stem-like cells, or i-cells, are localized on the basal side, called the tentacle bulb, while nematocytes are distributed as clusters on the distal side, similar to the jellyfish *Clytia* (Figures 1C, 2A, 3C and S3A-S3C) (Denker et al., 2008; Fujita et al., 2019; Hou et al., 2021). The existence of localized stem-like cells at the bulb prompted us to examine tentacle regeneration as a model for appendage regeneration in non-bilaterians.

***Cladonema* medusa tentacles functionally regenerate upon amputation**

When the tentacle was amputated with the bulb left intact (Figures 1D and 1E), wound closure finished by 24 hours post-amputation (hpa) (Figures S1A and S1B), at which point the injury site became smooth surface (Figures 1D i and 1D ii). Subsequently, tentacles began to elongate distally, and nematocyte clusters formed at the tip of the regenerating tentacle at 48 hpa (Figure 1D iii). The number of nematocyte clusters increased during tentacle elongation, and these clusters were localized along the distal side at 72 hpa, which is when the regenerating tentacle branched, a characteristic feature of the genus *Cladonema* (Figures 1D iv and 1E). Notably, these regeneration processes occurred without feeding, suggesting that tentacle regeneration is an immediate response for the organism to re-construct the organ that is required for capturing food.

346 To investigate the subtleties of tentacle morphology at cellular resolution during
347 regeneration, we visualized the muscle fibers, mature nematocytes, and neurons by
348 staining F-actin, poly-γ-glutamate, and FMRFamide and acetylated tubulin, respectively
349 (Figures 1F, 1G and S1C, S1D). During the early stages of regeneration (0-24 hpa),
350 wound closure occurred progressively via the accumulation of supra-cellular actin fibers
351 (Figures 1F i and 1F ii). Accordingly, muscle fibers regenerated during tentacle
352 elongation (Figures 1F iii and 1F iv). While mature nematocytes were rarely found in the
353 bulb or the injury site until 24 hpa (Figures 1F i and 1F ii), nematocytes began to
354 accumulate at the tip of the regenerating tentacle at 48 hpa and formed clusters at 72
355 hpa (Figures 1F iii and 1F iv). The re-formation of neurons on the distal side occurred at
356 48 hpa and completed at 72 hpa (Figures 1G and S1C, S1D). These results suggest
357 that the regenerating tentacle is fully functional after 48 hpa. To test this possibility, we
358 examined whether the regenerating tentacle is capable of feeding. While the
359 regenerating tentacle was not functional until 24 hpa, more than half of the regenerating
360 tentacles captured prey at 48 hpa (55%), and this ratio reached 100% at 72 hpa
361 (Figures 1H and 1I). These results indicate that *Cladonema* medusae can fully
362 regenerate a functional tentacle within 2-3 days of amputation.
363 While the *Cladonema* medusa tentacle can almost always regenerate with the
364 bulb left intact, it is unclear whether the tentacle can still regenerate even after the bulb
365 has been removed (Figure 1J i). We thus ablated the entire tentacle, including the bulb,
366 and monitored the regeneration process. After amputation, the ring canal and the radial
367 canal adhered, and the wound closure completed at 1 day post-amputation (dpa)
368 (Figure 1J ii). The injured area began to bulge as early as 5 dpa, and the transparent
369 wound site turned orange, which reflects the color of its food, *Artemia* (Figure 1J iii). The
370 *de novo* tentacle bulb reformed within 1-2 weeks with a nematocyte cluster at the tip,
371 and the small tentacle gradually elongated (Figures 1J iv and 1K). Because the rate of
372 successful regeneration varied dramatically while rearing medusae under the same
373 conditions and feeding frequency, tentacle bulb regeneration likely depends on the
374 health condition of the individual medusa (Figure S1E).
375 We also examined the regenerative potential of isolated tentacles. While the
376 whole body cannot be regrown from isolated tentacles in *Hydra* or *Nematostella* (Amiel
377 et al., 2019; Galliot et al., 2018), polyps in the jellyfish *Aurelia aurita* can regenerate

378 from isolated tentacles (Lesh-Laurie et al., 1991). To examine the regeneration capacity
379 of the isolated tentacle in *Cladonema*, we cultured *Cladonema* medusa tentacles either
380 with or without the bulb left intact. Although wound closure successfully occurred
381 regardless of the existence of the bulb, tissues and organs located to the proximal side
382 of the tentacle including the umbrella, the radial canal, and the bulb, did not regenerate,
383 and the isolated tentacle gradually degenerated (Figures S1F and S1G).
384 These observations together show that the *Cladonema* medusa tentacle can
385 functionally regenerate after amputation, but that its organ repair capacity is restricted to
386 the organism that recognizes the missing tentacle, likely through the canals, as
387 previously shown in the *Clytia* medusa (Sinigaglia et al., 2020). For our remaining
388 studies, we focused our attention on the process of tentacle regeneration with the bulb
389 intact, which provides a highly reproducible and tractable system.
390
391 **Blastema is formed in the early phase of tentacle regeneration**
392 During organ regeneration, blastema forms at the regenerating tip after wound closure
393 and contributes to reconstruction of the new tissue as a source of cell proliferation and
394 differentiation (McCusker et al., 2015; Seifert and Muneoka, 2018). In order to
395 investigate the timing of blastema formation during *Cladonema* tentacle regeneration,
396 we performed pulse labeling of EdU, a S-phase marker (Figure 2A) (Salic and
397 Mitchison, 2008). To understand the spatial pattern of cell proliferation, we defined
398 basal, middle, and distal regions in the regenerating tentacle and quantified the
399 distribution of proliferating cells. Consistent with the localization of stem-like cells
400 (Figure 3C i), cell proliferation in the intact tentacle was mainly detected on the basal
401 side (Figures 2A i and 2B). By contrast, cell proliferation in the regenerating tentacle
402 was frequently observed on the distal side near the wound area at 24 hpa (Figures 2A ii
403 and B). At 72 hpa, unlike at 24 and 48 hpa, cell proliferation was detected in the middle
404 and on basal side, not on the distal side (Figures 2A iv and 2B). We further confirmed
405 the pattern of proliferating cells using the M-phase marker, anti-Phospho-Histone 3
406 (PH3) antibody. While $PH3^+$ cells were distributed across the basal side before
407 amputation, in the regenerating tentacle, $PH3^+$ cells accumulated on the distal side at
408 24 hpa, and gradually localized on the basal side starting at 48 hpa (Figures 2D and
409 S2), which is consistent with the results of EdU^+ cell distribution (Figures 2A and 2B).

410 These results also reflect the fact that differentiated nematocytes accumulate on the
411 distal side at 48 hpa and 72 hpa (Figures 1D and 1F). Together, these observations
412 suggest that cell proliferation is accelerated near the injury site at 24 hpa after
413 amputation.
414 Blastema cells are undifferentiated cell populations that possess a high mitotic
415 capacity during regeneration (Tasaki et al., 2011). We thus investigated proliferative
416 activity in detail during the early phase of tentacle regeneration (Figures 2D-2F). In the
417 regenerating tip, the number of $PH3^+$ and EdU^+ cells was about 4 and 20 times greater,
418 respectively, than the corresponding area in the intact tentacle (Figures 2D-2F).
419 Moreover, these $PH3^+$ and EdU^+ cell numbers at the regenerating tip were significantly
420 greater than those in the bulb of the intact tentacle where stem-like cells are localized
421 (Figures 2D-2F). Notably, nearly half of the cells in the regenerating tip are EdU^+ cells
422 (Figures 2D ii and 2F). Altogether, these results indicate that proliferative activity in the
423 regenerating tip is much higher than that of cells not in the regenerating tip, which
424 provides evidence that blastema cells appear during tentacle regeneration.
425 To determine whether blastema formation is specific to the location of
426 amputation, we examined the localization of proliferating cells after dissecting tentacles
427 in different ways. When the distal side of the tentacle is amputated, ectopic cell
428 proliferation was observed near the injury site at 24 hpa (Figure 2G). Similarly, when the
429 tentacle was amputated with the bulb, cell proliferation occurred around the injury site
430 where the canals merged at 24 hpa (Figure 2H). These results suggest that blastema is
431 formed around the injury site regardless of the location of amputation.
432 Based on these observations, we hypothesized that blastema is prerequisite for
433 proper regeneration of the tentacle. To test this possibility, we examined whether
434 blastema formation occurs in the isolated tentacle, which fails to regenerate basal tissue
435 (Figure S1F). In the isolated tentacle, EdU^+ cells were not detected at the injury site at
436 24 hpa (Figure 2I). These results together suggest that blastema formation is
437 associated solely with the regenerating tentacle.
438
439 **Stem-like cells compose blastema**
440 What cell types constitute blastema? In hydrozoans, i-cells behave as pluri-/multipotent
441 stem cells that can differentiate into progenitors and differentiated lineages (Gold and

442 Jacobs, 2013). In order to confirm the cell types that form blastema, we utilized the
443 combination of β-catenin antibody staining and nuclear staining, which can distinguish i-
444 cells, nematocytes, and epithelial cells (Figure 3A). In both *Hydractinia* and *Cladonema*,
445 i-cells were identified by cytoplasmic signals of β-catenin, together with the large
446 nucleus-to-cytoplasm ratio and prominent nucleoli (Hou et al., 2021; Plickert et al.,
447 2012). While nematocytes exhibit crescent-shaped nuclei, epithelial cells show a
448 polygonal shape delineated by the membrane-localized β-catenin (Figure 3A iii).
449 Through the quantification of cell types, we found that around 80% of blastema cells
450 were i-cells, 10% were epithelial cells, and 10% were nematocytes (Figures 3A and 3B),
451 indicating that most cells in blastema are i-cells.
452 To molecularly characterize these blastema cells, we examined the expression
453 of the stem cell markers *Nanos1* and *Piwi* by fluorescent *in situ* hybridization (FISH). In
454 the intact tentacle, *Nanos1*$^+$ cells are primarily distributed in the bulb of the intact
455 tentacle (Fujita et al., 2022; Hou et al., 2021). By contrast, at 24 hpa *Nanos1*$^+$ cells
456 accumulated around the injury site where blastema formed (Figure 3C ii), and *Piwi*$^+$
457 cells were also localized in the blastema region (Figure S3C). While *Nanos1*$^+$ cells
458 accumulated to the new branching bud after 48 hpa (Figure 3C iii, Fujita et al., 2022;
459 Hou et al., 2021), *Nanos1* expression was no longer detected at the regenerating tip
460 and was restricted to the middle and basal side of the tentacle (Figure 3C iii). We further
461 quantified the distribution of *Nanos1*$^+$ cells and found a gradual transition of their
462 distribution from the distal to the basal side of the regenerating tentacle (Figure 3D).
463 These results are consistent with the distribution pattern of proliferative cells (Figures
464 2A-2C and S2), further supporting the idea that proliferative cells in blastema are stem-
465 like cells.
466
467 **Blastema cells are not derived from stem-like cells localized at the bulb**
468 Previous reports on cnidarian regeneration have suggested that undifferentiated
469 blastema cells are supplied by the migration of resident stem/progenitor cells in
470 response to injury (Amiel et al., 2019; Bradshaw et al., 2015; Sinigaglia et al., 2020). To
471 test whether resident stem cells, or originally-localized i-cells, in the bulb migrate to the
472 injury site to form blastema, we performed EdU-chase experiments during *Cladonema*
473 tentacle regeneration. We leveraged the fact that short-time incubation of EdU labels

474 proliferating i-cells in the intact tentacle, and, after incubating, amputated and visualized
475 the tentacle at different time points (Figure S4A i). At 24 hpa, EdU^+ cells remained fairly
476 distributed across the tentacle (Figure S4A ii). Following 48 h and 72 h chasing, EdU^+
477 cells continued to localize at the basal side, including the bulb, rather than in the
478 regenerating tip, although the population of EdU^+ cells propagated in the distal direction
479 likely through cell proliferation and migration (Figures S4A iii and S4A iv). We further
480 conducted an alternative tracing experiment that specifically labels cells in the bulb
481 region by DiI microinjection followed by amputation and cell tracking (Figures S4B and
482 S4C). After a 24 h chase, DiI^+ cells were still localized near the bulb (Figure S4C ii),
483 which, taken together with the EdU chase results, suggests that proliferating stem-like
484 cells do not migrate to the blastema region.
485 The above experiments support the presence of two populations of proliferative
486 cells during regeneration: one population are the "homeostatic proliferative cells,"
487 composed of stem-like cells localized at the bulb, and the other are "repair-specific
488 proliferative cells" that appear *de novo* as blastema upon amputation. In order to test
489 this hypothesis, we performed chasing experiments by labeling the two proliferative cell
490 populations with distinct nucleoside analogs, EdU and BrdU (Figure 4A). This approach
491 has been utilized in different animal systems as a way to track proliferative cell
492 populations and their lineages (Harris et al., 2018; Ribeiro et al., 2021; Vega and
493 Peterson, 2005). We labeled homeostatic proliferative cells in the bulb by EdU before
494 amputation and repair-specific proliferative cells in the blastema by BrdU at 24 hpa
495 (Figure 4A). At the time of blastema formation at 24 hpa, EdU^+ homeostatic proliferative
496 cells were still localized to the bulb, and only 12.6% merged with $BrdU^+$ cells, which
497 accumulated at the blastema (Figure 4B i). Following 24-48 h, $BrdU^+$ cells were
498 distributed on the distal side of the regenerating tentacle while EdU^+ cells remained
499 localized on the basal side, although their distribution expanded slightly (Figures 4B ii
500 and 4B iii). These results suggest that repair-specific proliferative cells at the blastema
501 participate in the formation of the new structure while homeostatic proliferative cells
502 expand locally, supporting the existence of two distinct proliferative cell populations
503 during tentacle regeneration (Figure 4E).
504 To determine the characteristics of these distinct proliferative cell populations,
505 we examined their respective proliferative capacities. For this purpose, we quantified

506 the increase in cell numbers of the two populations during tentacle regeneration. At 24
507 hpa, homeostatic proliferative cells increased approximately two-fold, but no significant
508 difference was observed in the following 48 h (Figure 4C; 0 hpa: n=161.2±13.5, 24 hpa:
509 n=392.2±32.1, 48 hpa: n=426.8±28.5, 72 hpa: n=385.7±29.1). Notably, the number of
510 these proliferative cells also increased during 24 h without amputation (Figures S4D and
511 S4E), suggesting that the increase of homeostatic proliferative cells is not an injury-
512 specific response. In contrast, the number of repair-specific proliferative cells in the
513 blastema tripled at 48 h, which led to an approximate 4-fold increase at 72 hpa (Figure
514 4D; 24 hpa: n=275.1±19.4, 48 hpa: n=929.3±45.8, 72 hpa: n=1125±100.7). These
515 results indicate a pronounced difference in proliferative activity between the two
516 populations, further implicating their distinct responses to injury.
517 If repair-specific proliferative cells do not derive from the resident stem-like cells
518 in the bulb, blastema should form when such stem-like cells are removed. To test this
519 possibility, we examined blastema formation after homeostatic proliferative cells are
520 eliminated by X-ray irradiation. We first confirmed the elimination of stem-like cells after
521 X-ray irradiation (30 Gy) by monitoring expression of the stem cell marker *Nanos1*.
522 qPCR analysis after X-ray irradiation revealed a gradual reduction of *Nanos1* mRNA
523 levels, particularly after 3 days post-irradiation (dpi) (Figure S5A). FISH staining of
524 *Nanos1* also showed that its signal in the bulb decreased significantly at 3 dpi (Figures
525 S5B and S5C). We thus amputated the tentacle at 3 dpi and investigated the blastema
526 formation by EdU pulse labeling (Figure 4F). At 24 hpa, blastema successfully formed
527 regardless of X-ray irradiation (Figure 4G). Of note, the rate of EdU^+ cells in the
528 blastema was equivalent between tentacles with X-ray irradiation and controls (Figure
529 4H). Combined, these results demonstrate that distinct proliferative cell populations
530 appear during tentacle regeneration and that blastema cells are not derived from
531 resident stem-like cells.
532
533 **Homeostatic proliferative cells contribute to nematogenesis and tentacle**
534 **elongation**
535 In the tentacles of hydrozoan medusae such as *Clytia* and *Cladonema*, proliferative i-
536 cells in the bulb are proposed to migrate from the basal to the distal side while
537 differentiating into nematocytes, which is known as the belt conveyor model

538 (Condamine et al., 2019; Denker et al., 2008; Fujita et al., 2019). Based on this
539 proposed model, we hypothesized that homeostatic proliferative cells in the bulb
540 contribute to nematogenesis during both homeostasis and regeneration. In order to test
541 this hypothesis, we performed EdU and BrdU double chase experiments with some
542 modifications. We found that long-incubation with EdU for 24 h allows for the labeling of
543 most proliferative cells in the bulb as well as nematocyte progenitors labeled by *Mcol*
544 and *Nowa* (Figures 5B i and S6A-S6C). After EdU labeling for 24 h, followed by
545 amputation, most EdU^+ cells remained in the bulb and did not merge with repair-specific
546 proliferative cells labeled with BrdU in the blastema (Figure 5B ii), which is consistent
547 with the results of the chasing experiment using EdU pulse labeling (Figure 4B). At 72
548 hpa, while EdU^+ cells were still distributed in the basal region, including the bulb, some
549 EdU^+ cells were located in the distal nematocyte clusters (Figure 5B iii: yellow arrow),
550 suggesting that one of the lineages of homeostatic proliferative cells are nematocytes
551 during regeneration. To further confirm the above observation, we identified cell types
552 located in the distal side of the tentacle. We found that atypical protein kinase C (aPKC)
553 antibody can be utilized to detect cell types with nuclear staining, which is a method
554 similar to using β-catenin antibody (Figures 3A, 5C ii, and S7) (Hou et al., 2021; Plickert
555 et al., 2012). The combination of EdU chasing and cell type identification revealed that
556 nearly half of the EdU^+ cells are nematocytes in the distal side of the tentacle
557 (nematocytes: 45.7%, epithelial cells: 24.2%, i-cells: 30.1%; Figures 5C and 5D). These
558 results together indicate that homeostatic proliferative cells in the bulb differentiate into
559 nematocytes during regeneration.
560 Given that the homeostatic proliferative cells differentiate into both nematocytes
561 and epithelial cells during regeneration (Figures 5C and 5D), it is expected that these
562 cells play a role in supplying new nematocytes as well as in tentacle elongation. We first
563 examined the number of nematocytes when the homeostatic proliferative cells were
564 eliminated by X-ray (Figure 5E). At 72 hpa, the number of nematocyte clusters and
565 particularly stenoteles, large rugby ball-shaped nematocytes, were significantly reduced
566 in the X-ray irradiated medusae tentacles (nematocyte clusters, control: 11.7, X-ray:
567 6.52; stenoteles, control: 47.8, X-ray: 26.8) (Figures 5F-5H), indicating that homeostatic
568 proliferative cells migrate from the basal to the distal side while differentiating into
569 nematocytes during regeneration.

570 Next, we measured tentacle length during regeneration with homeostatic
571 proliferative cells removed by X-ray irradiation (Figure 5I). When tentacles were
572 amputated at 3 dpi and 5 dpi, by which time homeostatic proliferative cells had been
573 eliminated, tentacle elongation was significantly inhibited compared to the non-irradiated
574 controls (Figure 5J, regenerated tentacle length at 96 hpa, Control: 1.70mm, 1 dpi:
575 1.44mm, 3 dpi: 0.928mm, 5 dpi: 1.04mm). Although we cannot exclude the possibility
576 that X-ray irradiation affects the source of repair-specific proliferative cells to some
577 extent, we confirmed that EdU^+ blastema cells appear after X-ray irradiation (Figures 4G
578 and 4H), suggesting that homeostatic proliferative cells contribute to tentacle elongation
579 independently of blastema cells. We speculate that homeostatic proliferative cells, and
580 particularly their decedents, participate in tissue elongation likely through pushing out
581 from the basal side as progenitors and differentiating into epithelial cells.
582
583 **Repair-specific proliferative cells contribute to reconstruction of the new tentacle**
584 In order to investigate the role of repair-specific proliferative cells during regeneration,
585 we performed EdU pulse labeling of the blastema with cell type identification by aPKC
586 antibody staining (Figure 5K). While 94.4% of the injury-responsive proliferative cells
587 exhibited i-cell morphology at 24 hpa (Figures 5L i and 5M, consistent with the results of
588 β-catenin antibody staining in Figures 3A and 3B), 59.2% of EdU^+ cells were epithelial
589 cells in the distal portion of the regenerating tentacle at 72 hpa, (Figures 5L ii and 5M).
590 Strikingly, in contrast to homeostatic proliferative cells, EdU^+ cells derived from the
591 blastema did not become nematocytes (Figures 5A-5D and 5K-5M). These results
592 suggest that repair-specific proliferative cells preferentially differentiate into epithelial
593 cells in the regenerating tentacle.
594 To identify the role of repair-specific proliferative cells, we examined the impact
595 of locally inhibiting cell proliferation on tentacle regeneration (Figure 5N). UVA radiation
596 (320 to 400 nm) induces various forms of cellular damage via the production of reactive
597 oxygen species or the impairment of proteasomal function, which blocks cell cycle
598 progression at the G_2/M phase in both mammalian cultured cells and fly epidermal
599 progenitors (Catalgol et al., 2009; Girard et al., 2008; Latonen and Laiho, 2005;
600 Nakajima et al., 2011). In addition, Hoechst and BrdU are known photosensitizers
601 (Herweijer et al., 1988; Singh et al., 2004), which can facilitate the process of damage

602 induction. To verify the effects of UVA on the repair-specific proliferative cells, we
603 performed UV laser illumination around the blastema region at 24 hpa and counted the
604 number of EdU labeled cells (Figure S8). Following 24 h, the number of EdU^+ cells
605 decreased significantly in the UV exposed tentacle compared to the control, indicating
606 that UV laser exposure inhibits cell proliferation (Figure S8). In order to examine the
607 contribution of the proliferation of repair-specific proliferative cells toward tentacle
608 regeneration, we monitored the length of regenerating tentacles after UV laser exposure
609 (Figure 5N). Upon UV laser illumination, tentacle elongation during regeneration was
610 significantly inhibited (Figures 5N and 5O). These results, together with the distribution
611 of their descendants on the distal side of the regenerating tentacle (Figures 4B and 5B),
612 indicate that proliferation of repair-specific proliferative cells contribute to the
613 reconstruction of new tentacles after amputation.
614
615
616 ## Discussion
617 In this study, we uncovered the cellular mechanism underlying blastema formation
618 during *Cladonema* tentacle regeneration. We found that, upon amputation of the
619 tentacle, repair-specific proliferative cells accumulate as blastema, which is not derived
620 from resident i-cells. While resident i-cells contribute to nematogenesis and tissue
621 elongation during both homeostasis and regeneration, repair-specific proliferative cells
622 differentiate into the epithelial cells of the newly formed tentacle. Based on these
623 results, we propose that distinct proliferative cell populations facilitate rapid functional
624 regeneration of the tentacle, which enables critical behaviors of jellyfish organismal
625 physiology such as feeding and swimming (Figure 6A).
626
627 **Heterogeneity of i-cells**
628 In hydrozoans, i-cells behave as pluripotent stem cells that can differentiate into several
629 progenitors and differentiated lineages such as nematocytes, neurons, gland cells, and
630 gametes. Although i-cells exhibit common features such as their interstitial localization,
631 cellular morphology, and expression of the conserved stem cell markers (*Nanos, Piwi,*
632 *Vasa, PL10*); their potency and heterogeneity likely differ across species (Gold and
633 Jacobs, 2013). Indeed, *Hydra* i-cells differentiate into most cell types except epithelial

634 cells, while *Hydractinia* i-cells behave as pluripotent cells that can differentiate into all
635 cell types including somatic and germline cells (Watanabe et al., 2009; Gahan et al.,
636 2016; Varley et al., 2022).
637 In the intact *Cladonema* jellyfish, *Nanos1*$^{+}$ and *Piwi*$^{+}$ cells are primarily distributed
638 at the bulb (Figures 3C and S3), and about 70% of homeostatic proliferative cells in the
639 bulb are *Nanos1*$^{+}$ i-cells (Figures 3E and 3F). From lineage-tracing experiments, these
640 homeostatic proliferative cells differentiate into epithelia as well as nematocytes
641 (Figures 5C and 5D), suggesting their role as multipotent stem cells. These
642 observations are consistent with the jellyfish *Clytia*, in which i-cells in the bulb proliferate
643 and differentiate into nematocytes (Condamine et al., 2019; Denker et al., 2008),
644 indicating that i-cells in the tentacle bulb are commonly involved in organ homeostasis
645 including nematogenesis in hydrozoan jellyfish.
646 In contrast to i-cells in the bulb, only about 30% of repair-specific proliferative
647 cells at blastema express *Nanos1*$^{+}$ and *Piwi*$^{+}$*,* although more than 80% of blastema cells
648 show i-cell morphology (Figures 3A, B and 5L, 5M). These results imply that the i-cell
649 population of the blastema differs from that of resident i-cells in the bulb. Indeed, repair-
650 specific proliferative cells predominantly differentiate into epithelial cells rather than
651 nematocytes (Figures 5K-5M), suggesting their role as unipotent stem/progenitor cells.
652 Such repair-specific proliferative cells also accumulate at the newly-formed branch
653 starting at 48 hpa (Figure 4B), consistent with the prediction by the previous report
654 proposing that i-cell population in the branching bud differs from resident i-cells in the
655 bulb (Hou et al., 2021). Altogether, our findings support the heterogeneity of i-cells in
656 *Cladonema* jellyfish (Figure 6A), which is similar to the subpopulations of *Hydra* i-cells
657 (David, 2012; Govindasamy et al., 2014).
658
659 **How are repair-specific proliferative cells supplied in the blastema?**
660 Our work is the first to demonstrate that repair-specific proliferative cells appear upon
661 injury in cnidarians, but how this cell population is supplied remains unknown. Lineage-
662 tracing experiments show that blastema formation is independent of resident i-cells in
663 the bulb (Figures 4A-4E). When the distal side of the tentacle, where few proliferating
664 cells exist, is amputated, local cell proliferation is still observed around the injury site

665 (Figure 2G). These observations raise two possibilities: mitotic re-entry of
666 quiescent/slow-cycling i-cells or dedifferentiation from differentiated cells into i-cells.
667 Previous reports have showed that some cnidarian species possess quiescent or
668 slow-cycling stem cells. For instance, while *Hydra* has three types of adult stem cells—i-
669 cells, ectodermal stem cells, and endoderm epithelial stem cells—the subpopulation of
670 each stem cell is slow-cycling (Govindasamy et al., 2014). These slow-cycling cells are
671 resistant to hydroxyurea treatment due to G2 phase arrest, and re-enter the cell cycle
672 during head regeneration. *Nematostella* also has slow-cycling/quiescent cells that are
673 predominantly present in the mesenteries and are resistant to X-ray irradiation, and
674 these cells' cell cycle is activated upon injury, when they migrate toward the wound site
675 (Amiel et al., 2019). Given that a small number of i-cells exist in the *Cladonema* intact
676 tentacle, outside the bulb, and branching bud (Figure S3A) (Hou et al., 2021); such a
677 minor population of i-cells may behave as slow-cycling/quiescent cells and re-enter the
678 cell cycle in response to injury.
679 By contrast, although cnidarian dedifferentiation potential is still debated, some
680 species appear to exhibit context-dependent cellular plasticity (Nakanishi and Jacobs,
681 2019). For instance, classical experiments using the hydrozoan jellyfish *Podocoryna*
682 *carnea* have indicated their dedifferentiation potential *in vitro*: when isolated striated
683 muscles are cultured after collagenase treatment, the muscle cells dedifferentiate into
684 stem-like cells and re-differentiate into multiple cell types (Schmid and Alder, 1984).
685 Additionally, in green *Hydra*, the isolated gastrodermis, which is i-cell free, can
686 reconstitute a complete polyp including the ectoderm (Haynes and Burnett, 1963). In
687 this case, endodermal gland cells appear to dedifferentiate into i-cells (Burnett et al.,
688 1966), while endodermal digestive cells transdifferentiate into epidermal
689 epitheliomuscular cells (Davis et al., 1966). Moreover, a recent report using *Hydractinia*
690 has shown that, when the hypostome is isolated from the body, cellular reprogramming
691 triggered by cell senescence occurs in somatic cells, which convert into pluripotent
692 *Piwi1*$^{+}$ i-cells (Salinas-Saavedra et al., 2022). Although these reports support the
693 possibility that dedifferentiation produces pluri/multipotent stem cells after isolation from
694 the body, it is also possible that repair-specific proliferative cells are derived from their
695 descendant cell types. During newt limb regeneration, cellular lineage is restricted such
696 that muscle progenitors dedifferentiated from resident muscle fibers produce only

697 muscles (Sandoval-Guzmán et al., 2014; Tanaka et al., 2016). Given that repair-specific
698 proliferative cells in the *Cladonema* tentacle differentiate into only epithelial cells
699 (Figures 5K-5M), epithelial cells may dedifferentiate into unipotent progenitors that give
700 rise to only epithelial cells in the newly formed tentacle.
701
702 **Evolutionary conservation and diversification of blastema formation**
703 Although the molecular and cellular mechanisms of animal regeneration have been
704 addressed in detail using representative species such as planaria and salamanders,
705 questions such as the evolutionary history of regeneration and the homology of
706 regeneration mechanisms across species remain largely unknown. Repair-specific stem
707 cells provided by quiescent stem cells and/or dedifferentiation are common blastema
708 components in bilaterian appendage regeneration. As in vertebrates where lineage-
709 restricted repair-specific stem/progenitor cells participate in appendage regeneration
710 (Ando et al., 2017; Knopf et al., 2011; Lehoczky et al., 2011; Sandoval-Guzmán et al.,
711 2014), the protostome ecdysozoa *Parhyale hawaiensis* utilize re-activation of muscle
712 satellite cells during thoracic leg regeneration (Konstantinides and Averof, 2014). By
713 contrast, during echinoderm starfish arm regeneration, dedifferentiated dermal cells
714 form blastema-like structures (Fan et al., 2011). Similarly, during insect cricket leg
715 regeneration, the source of blastemal cells is derived from injury-induced
716 dedifferentiation (Bando et al., 2018; Truby, 1983). These reports suggest that repair-
717 specific production of blastema cells is relatively conserved throughout bilaterians
718 (Figure 6B).
719 In non-bilaterian metazoans, resident pluripotent stem cells are thought to
720 contribute to both homeostasis and whole-body regeneration. During the regeneration
721 of the demosponge in Porifera, one of the most primitive animals, archeocytes known
722 as homeostatic stem cells contribute to an undifferentiated cell mass beneath the
723 wound as a blastema-like structure (Borisenko et al., 2015). While the regenerating
724 ctenophore cydippids do not apparently form blastema-like structure, slow-cycling stem-
725 like cells are recruited to the injury site (Ramon-Mateu et al., 2019). In cnidarians,
726 resident stem cells, which are involved in homeostasis, are recruited to the injury site
727 after amputation of the body and removal of the organs (Amiel et al., 2019; Bradshaw et
728 al., 2015; Chera et al., 2009; Sinigaglia et al., 2020). By contrast, as shown in this study,

729 the source of blastemal cells are not resident i-cells but rather repair-specific
730 proliferative cells during *Cladonema* tentacle regeneration (Figure 4). Our findings
731 suggest that, in terms of the regeneration processes and blastemal cellular source, the
732 regeneration mechanism of the *Cladonema* tentacle is more homologous to that of
733 bilaterian species (Figure 6B).
734 One important remaining question is whether bilaterians' and cnidarians' most
735 recent common ancestor possessed a system to supply blastema through repair-
736 specific proliferative cells. Although sponges and ctenophores have been proposed to
737 possess dedifferentiation or transdifferentiation potentials that can provide a cellular
738 source of regenerated bodies (Nakanishi and Jacobs, 2019), it is currently unknown
739 whether they are repair-specific cell populations or not. In this study, we demonstrate
740 that repair-specific proliferative cells contribute to the newly generated epithelium during
741 *Cladonema* tentacle regeneration. Intriguingly, recent genomic studies have revealed
742 that jellyfish-specific genes are not conserved among bilaterians or even other
743 cnidarians including corals and sea anemones, and the anthozoan *Nematostella* is the
744 most 'bilaterian-like' cnidarian sequenced (Khalturin et al., 2019; Putnam et al., 2007;
745 Steele et al., 2011). These findings raise the possibility that medusozoans had evolved
746 the medusa stage after branching from their common ancestor and that bilaterians and
747 cnidarian jellyfish likely independently acquired a similar mechanism of blastema
748 formation upon amputation of appendages. It is thus tempting to speculate that
749 blastema formation by repair-specific proliferative cells is a common feature acquired for
750 complex organ and appendage regeneration during animal evolution.
751
752

753 ## References

754 Amiel AR, Foucher K, Ferreira S, Röttinger E. 2019. Synergic coordination of stem cells is
755 required to induce a regenerative response in anthozoan cnidarians.
756 doi:10.1101/2019.12.31.891804

757 Ando K, Shibata E, Hans S, Brand M, Kawakami A. 2017. Osteoblast Production by Reserved
758 Progenitor Cells in Zebrafish Bone Regeneration and Maintenance. *Developmental Cell* **43**:643-
759 650.e3. doi:10.1016/j.devcel.2017.10.015

760 Aztekin C. 2021. Appendage regeneration is context dependent at the cellular level. *Open Biol*
761 **11**:210126. doi:10.1098/rsob.210126

762 Bando T, Mito T, Hamada Y, Ishimaru Y, Noji S, Ohuchi H. 2018. Molecular mechanisms of
763 limb regeneration: insights from regenerating legs of the cricket Gryllus bimaculatus. *Int J Dev*
764 *Biol* **62**:559–569. doi:10.1387/ijdb.180048ho

765 Bely AE, Nyberg KG. 2010. Evolution of animal regeneration: re-emergence of a field. *Trends*
766 *in Ecology & Evolution* **25**:161–170. doi:10.1016/j.tree.2009.08.005

767 Borisenko IE, Adamska M, Tokina DB, Ereskovsky AV. 2015. Transdifferentiation is a driving
768 force of regeneration in *Halisarca dujardini* (Demospongiae, Porifera). *PeerJ* **3**:e1211.
769 doi:10.7717/peerj.1211

770 Bradshaw B, Thompson K, Frank U. 2015. Distinct mechanisms underlie oral vs aboral
771 regeneration in the cnidarian Hydractinia echinata. *eLife* **4**:e05506. doi:10.7554/eLife.05506

772 Burnett AL, Davis LE, Ruffing FE. 1966. A histological and ultrastructural study of germinal
773 differentiation of interstitial cells arising from gland cells inHydra viridis. *J Morphol* **120**:1–8.
774 doi:10.1002/jmor.1051200102

775 Catalgol B, Ziaja I, Breusing N, Jung T, Höhn A, Alpertunga B, Schroeder P, Chondrogianni N,
776 Gonos ES, Petropoulos I, Friguet B, Klotz L-O, Krutmann J, Grune T. 2009. The Proteasome Is
777 an Integral Part of Solar Ultraviolet A Radiation-induced Gene Expression. *Journal of Biological*
778 *Chemistry* **284**:30076–30086. doi:10.1074/jbc.M109.044503

779 Chera S, Ghila L, Dobretz K, Wenger Y, Bauer C, Buzgariu W, Martinou J-C, Galliot B. 2009.
780 Apoptotic Cells Provide an Unexpected Source of Wnt3 Signaling to Drive Hydra Head
781 Regeneration. *Developmental Cell* **17**:279–289. doi:10.1016/j.devcel.2009.07.014

782 Condamine T, Jager M, Leclère L, Blugeon C, Lemoine S, Copley RR, Manuel M. 2019.
783 Molecular characterisation of a cellular conveyor belt in Clytia medusae. *Developmental Biology*
784 **456**:212–225. doi:10.1016/j.ydbio.2019.09.001

785 Daponte V, Tylzanowski P, Forlino A. 2021. Appendage Regeneration in Vertebrates: What
786 Makes This Possible? *Cells* **10**:242. doi:10.3390/cells10020242

787 David CN. 2012. Interstitial stem cells in Hydra: multipotency and decision-making. *Int J Dev*
788 *Biol* **56**:489–497. doi:10.1387/ijdb.113476cd

789 Davis LE, Burnett AL, Haynes JF, Mumaw VR. 1966. A histological and ultrastructural study of
790 dedifferentiation and redifferentiation of digestive and gland cells in Hydra viridis.
791 *Developmental Biology* **14**:307–329. doi:10.1016/0012-1606(66)90018-2

792 Denker E, Manuel M, Leclère L, Le Guyader H, Rabet N. 2008. Ordered progression of
793 nematogenesis from stem cells through differentiation stages in the tentacle bulb of Clytia
794 hemisphaerica (Hydrozoa, Cnidaria). *Developmental Biology* **315**:99–113.
795 doi:10.1016/j.ydbio.2007.12.023

796 Fan T, Fan X, Du Y, Sun W, Zhang S, Li J. 2011. Patterns and cellular mechanisms of arm
797 regeneration in adult starfish Asterias rollestoni bell. *J Ocean Univ China* **10**:255–262.
798 doi:10.1007/s11802-011-1837-y

799 Fritz AE, Ikmi A, Seidel C, Paulson A, Gibson MC. 2013. Mechanisms of tentacle
800 morphogenesis in the sea anemone *Nematostella vectensis*. *Development* **140**:2212–2223.
801 doi:10.1242/dev.088260

802 Fujiki A. 2019. Branching pattern and morphogenesis of medusa tentacles in the jellyfish
803 Cladonema pacificum (Hydrozoa, Cnidaria). *Zoological Letters* **5**:13. doi:10.1186/s40851-019-
804 0124-4

805 Fujita S, Kuranaga E, Miura M, Nakajima Y-I. 2022. Fluorescent In Situ Hybridization and 5-
806 Ethynyl-2'-Deoxyuridine Labeling for Stem-like Cells in the Hydrozoan Jellyfish Cladonema
807 pacificum. *J Vis Exp*. doi:10.3791/64285

808 Fujita S, Kuranaga E, Nakajima Y. 2021. Regeneration Potential of Jellyfish: Cellular
809 Mechanisms and Molecular Insights. *Genes* **12**:758. doi:10.3390/genes12050758

810 Fujita S, Kuranaga E, Nakajima Y. 2019. Cell proliferation controls body size growth, tentacle
811 morphogenesis, and regeneration in hydrozoan jellyfish *Cladonema pacificum*. *PeerJ* **7**:e7579.
812 doi:10.7717/peerj.7579

813 Gahan JM, Bradshaw B, Flici H, Frank U. 2016. The interstitial stem cells in Hydractinia and
814 their role in regeneration. *Current Opinion in Genetics & Development* **40**:65–73.
815 doi:10.1016/j.gde.2016.06.006

816 Galliot B, Buzgariu W, Schenkelaars Q, Wenger Y. 2018. Non-developmental dimensions of
817 adult regeneration in Hydra. *Int J Dev Biol* **62**:373–381. doi:10.1387/ijdb.180111bg

818 Gamero-Mora E, Halbauer R, Bartsch V, Stampar SN, Morandini AC. 2019. Regenerative
819 Capacity of the Upside-down Jellyfish Cassiopea xamachana. *Zool Stud* **58**.
820 doi:10.6620/ZS.2019.58-37

821 Girard P-M, Pozzebon M, Delacôte F, Douki T, Smirnova V, Sage E. 2008. Inhibition of S-phase
822 progression triggered by UVA-induced ROS does not require a functional DNA damage
823 checkpoint response in mammalian cells. *DNA Repair* **7**:1500–1516.
824 doi:10.1016/j.dnarep.2008.05.004

825 Gold DA, Jacobs DK. 2013. Stem cell dynamics in Cnidaria: are there unifying principles? *Dev*
826 *Genes Evol* **223**:53–66. doi:10.1007/s00427-012-0429-1

827 Govindasamy N, Murthy S, Ghanekar Y. 2014. Slow-cycling stem cells in hydra contribute to
828 head regeneration. *Biology Open* **3**:1236–1244. doi:10.1242/bio.201410512

829 Harris L, Zalucki O, Piper M. 2018. BrdU/EdU dual labeling to determine the cell-cycle
830 dynamics of defined cellular subpopulations. *J Mol Hist* **49**:229–234. doi:10.1007/s10735-018-
831 9761-8

832 Haynes J, Burnett AL. 1963. Dedifferentiation and Redifferentiation of Cells in Hydra viridis.
833 *Science* **142**:1481–1483. doi:10.1126/science.142.3598.1481

834 Herweijer H, And WS, Visser JWM. 1988. High-speed photodamage cell selection using
835 bromodeoxyuridine/Hoechst 33342 photosensitized cell killing. *Cytometry* **9**:143–149.
836 doi:10.1002/cyto.990090208

837 Holstein TW, Hobmayer E, Technau U. 2003. Cnidarians: An evolutionarily conserved model
838 system for regeneration? *Dev Dyn* **226**:257–267. doi:10.1002/dvdy.10227

839 Hou S, Zhu J, Shibata S, Nakamoto A, Kumano G. 2021. Repetitive accumulation of interstitial
840 cells generates the branched structure of *Cladonema* medusa tentacles. *Development*
841 **148**:dev199544. doi:10.1242/dev.199544

842 Katsuki T, Greenspan RJ. 2013. Jellyfish nervous systems. *Current Biology* **23**:R592–R594.
843 doi:10.1016/j.cub.2013.03.057

844 Khalturin K, Shinzato C, Khalturina M, Hamada M, Fujie M, Koyanagi R, Kanda M, Goto H,
845 Anton-Erxleben F, Toyokawa M, Toshino S, Satoh N. 2019. Medusozoan genomes inform the
846 evolution of the jellyfish body plan. *Nat Ecol Evol* **3**:811–822. doi:10.1038/s41559-019-0853-y

847 Knopf F, Hammond C, Chekuru A, Kurth T, Hans S, Weber CW, Mahatma G, Fisher S, Brand
848 M, Schulte-Merker S, Weidinger G. 2011. Bone Regenerates via Dedifferentiation of Osteoblasts
849 in the Zebrafish Fin. *Developmental Cell* **20**:713–724. doi:10.1016/j.devcel.2011.04.014

850 Konstantinides N, Averof M. 2014. A Common Cellular Basis for Muscle Regeneration in
851 Arthropods and Vertebrates. *Science* **343**:788–791. doi:10.1126/science.1243529

852 Latonen L, Laiho M. 2005. Cellular UV damage responses—Functions of tumor suppressor p53.
853 *Biochimica et Biophysica Acta (BBA) - Reviews on Cancer* **1755**:71–89.
854 doi:10.1016/j.bbcan.2005.04.003

855 Leclère L, Röttinger E. 2017. Diversity of Cnidarian Muscles: Function, Anatomy, Development
856 and Regeneration. *Front Cell Dev Biol* **4**. doi:10.3389/fcell.2016.00157

857 Lehoczky JA, Robert B, Tabin CJ. 2011. Mouse digit tip regeneration is mediated by fate-
858 restricted progenitor cells. *Proc Natl Acad Sci USA* **108**:20609–20614.
859 doi:10.1073/pnas.1118017108

860 Lesh-Laurie GE, Hujer A, Suchy P. 1991. Polyp regeneration from isolated tentacles of Aurelia
861 scyphistomae: a role for gating mechanisms and cell division. *Hydrobiologia* **216**:91–97.
862 doi:10.1007/BF00026448

863 Masuda-Ozawa T, Fujita S, Nakamura R, Watanabe H, Kuranaga E, Nakajima Y. 2022. siRNA-
864 mediated gene knockdown via electroporation in hydrozoan jellyfish embryos. *Sci Rep*
865 **12**:16049. doi:10.1038/s41598-022-20476-1

866 McCusker C, Bryant SV, Gardiner DM. 2015. The axolotl limb blastema: cellular and molecular
867 mechanisms driving blastema formation and limb regeneration in tetrapods: The Axolotl Limb
868 Blastema. *Regeneration* **2**:54–71. doi:10.1002/reg2.32

869 Nakajima Y, Kuranaga E, Sugimura K, Miyawaki A, Miura M. 2011. Nonautonomous Apoptosis
870 Is Triggered by Local Cell Cycle Progression during Epithelial Replacement in Drosophila. *Mol*
871 *Cell Biol* **31**:2499–2512. doi:10.1128/MCB.01046-10

872 Nakanishi N, Jacobs DK. 2019. The Early Evolution of Cellular Reprogramming in Animals In:
873 Bishop CD, Hall BK, editors. Deferring Development. CRC Press. pp. 67–86.
874 doi:10.1201/9780429445446-4

875 Ostendarp M, Plewka J, Flathmann J, Tilstra A, El-Khaled YC, Wild C. 2022. Complete and
876 rapid regeneration of fragments from the upside-down jellyfish Cassiopea. *Front Mar Sci*
877 **9**:949233. doi:10.3389/fmars.2022.949233

878 Passamaneck YJ, Martindale MQ. 2012. Cell proliferation is necessary for the regeneration of
879 oral structures in the anthozoan cnidarian Nematostella vectensis. *BMC Dev Biol* **12**:34.
880 doi:10.1186/1471-213X-12-34

881 Plickert G, Frank U, Müller WA. 2012. Hydractinia, a pioneering model for stem cell biology
882 and reprogramming somatic cells to pluripotency. *Int J Dev Biol* **56**:519–534.
883 doi:10.1387/ijdb.123502gp

884 Putnam NH, Srivastava M, Hellsten U, Dirks B, Chapman J, Salamov A, Terry A, Shapiro H,
885 Lindquist E, Kapitonov VV, Jurka J, Genikhovich G, Grigoriev IV, Lucas SM, Steele RE,
886 Finnerty JR, Technau U, Martindale MQ, Rokhsar DS. 2007. Sea Anemone Genome Reveals
887 Ancestral Eumetazoan Gene Repertoire and Genomic Organization. *Science* **317**:86–94.
888 doi:10.1126/science.1139158

889 Ramon-Mateu J, Ellison ST, Angelini TE, Martindale MQ. 2019. Regeneration in the ctenophore
890 Mnemiopsis leidyi occurs in the absence of a blastema, requires cell division, and is temporally
891 separable from wound healing. *BMC Biol* **17**:80. doi:10.1186/s12915-019-0695-8

892 Reddien PW, Alvarado AS. 2004. FUNDAMENTALS OF PLANARIAN REGENERATION.
893 *Annu Rev Cell Dev Biol* **20**:725–757. doi:10.1146/annurev.cellbio.20.010403.095114

894 Rees JT. 1979. The polyp and immature medusa stages of *Cladonema californicum* , Hyman,
895 1947 (Anthomedusae: Cladonemidae) with biological notes and a discussion of the taxonomy of
896 the genus *Cladonema*. *Journal of Natural History* **13**:295–302.
897 doi:10.1080/00222937900770231

898 Ribeiro RP, Egger B, Ponz-Segrelles G, Aguado MT. 2021. Cellular proliferation dynamics
899 during regeneration in Syllis malaquini (Syllidae, Annelida). *Front Zool* **18**:27.
900 doi:10.1186/s12983-021-00396-y

901 Röttinger E. 2021. Nematostella vectensis, an Emerging Model for Deciphering the Molecular
902 and Cellular Mechanisms Underlying Whole-Body Regeneration. *Cells* **10**:2692.
903 doi:10.3390/cells10102692

904 Salic A, Mitchison TJ. 2008. A chemical method for fast and sensitive detection of DNA
905 synthesis *in vivo*. *Proc Natl Acad Sci USA* **105**:2415–2420. doi:10.1073/pnas.0712168105

906 Salinas-Saavedra M, Febrimarsa, Krasovec G, Horkan HR, Baxevanis AD, Frank U. 2022.
907 Senescence-induced cellular reprogramming drives cnidarian whole-body regeneration.
908 doi:10.1101/2022.09.02.506310

909 Sandoval-Guzmán T, Wang H, Khattak S, Schuez M, Roensch K, Nacu E, Tazaki A, Joven A,
910 Tanaka EM, Simon A. 2014. Fundamental Differences in Dedifferentiation and Stem Cell
911 Recruitment during Skeletal Muscle Regeneration in Two Salamander Species. *Cell Stem Cell*
912 **14**:174–187. doi:10.1016/j.stem.2013.11.007

913 Schmid V, Alder H. 1984. Isolated, mononucleated, striated muscle can undergo pluripotent
914 transdifferentiation and form a complex regenerate. *Cell* **38**:801–809. doi:10.1016/0092-
915 8674(84)90275-7

916 Seifert AW, Muneoka K. 2018. The blastema and epimorphic regeneration in mammals.
917 *Developmental Biology* **433**:190–199. doi:10.1016/j.ydbio.2017.08.007

918 Singh S, Dwarakanath B, Mathew T. 2004. DNA ligand Hoechst-33342 enhances UV induced
919 cytotoxicity in human glioma cell lines. *Journal of Photochemistry and Photobiology B: Biology*
920 **77**:45–54. doi:10.1016/S1011-1344(04)00122-8

921 Sinigaglia C, Peron S, Eichelbrenner J, Chevalier S, Steger J, Barreau C, Houliston E, Leclère L.
922 2020. Pattern regulation in a regenerating jellyfish. *eLife* **9**:e54868. doi:10.7554/eLife.54868

923 Stamatis S-A, Worsaae K, Garm A. 2018. Regeneration of the Rhopalium and the Rhopalial
924 Nervous System in the Box Jellyfish *Tripedalia cystophora*. *The Biological Bulletin* **234**:22–36.
925 doi:10.1086/697071

926 Steele RE, David CN, Technau U. 2011. A genomic view of 500 million years of cnidarian
927 evolution. *Trends in Genetics* **27**:7–13. doi:10.1016/j.tig.2010.10.002

928 Stierwald M, Yanze N, Bamert RP, Kammermeier L, Schmid V. 2004. The Sine oculis/Six class
929 family of homeobox genes in jellyfish with and without eyes: development and eye regeneration.
930 *Developmental Biology* **274**:70–81. doi:10.1016/j.ydbio.2004.06.018

931 Suga H, Schmid V, Gehring WJ. 2008. Evolution and Functional Diversity of Jellyfish Opsins.
932 *Current Biology* **18**:51–55. doi:10.1016/j.cub.2007.11.059

933 Takeda N, Kon Y, Artigas GQ, Lapébie P, Barreau C, Koizumi O, Kishimoto T, Tachibana K,
934 Houliston E, Deguchi R. 2018. Identification of jellyfish neuropeptides that act directly as oocyte
935 maturation-inducing hormones. *Development* **145**. doi:10.1242/dev.156786

936 Tanaka EM, Reddien PW. 2011. The Cellular Basis for Animal Regeneration. *Developmental*
937 *Cell* **21**:172–185. doi:10.1016/j.devcel.2011.06.016

938 Tanaka HV, Ng NCY, Yang Yu Z, Casco-Robles MM, Maruo F, Tsonis PA, Chiba C. 2016. A
939 developmentally regulated switch from stem cells to dedifferentiation for limb muscle
940 regeneration in newts. *Nat Commun* **7**:11069. doi:10.1038/ncomms11069

941 Tasaki J, Shibata N, Sakurai T, Agata K, Umesono Y. 2011. Role of c-Jun N-terminal kinase
942 activation in blastema formation during planarian regeneration: JNK activation in planarian
943 regeneration. *Development, Growth & Differentiation* **53**:389–400. doi:10.1111/j.1440-
944 169X.2011.01254.x

945 Technau U, Steele RE. 2011. Evolutionary crossroads in developmental biology: Cnidaria.
946 *Development* **138**:1447–1458. doi:10.1242/dev.048959

947 Truby PR. 1983. Blastema formation and cell division during cockroach limb regeneration.
948 *Development* **75**:14.

949 Varley Á, Horkan HR, McMahon ET, Krasovec G, Frank U. 2022. Pluripotent, germ cell
950 competent adult stem cells underlie cnidarian plant-like life history (preprint). Developmental
951 Biology. doi:10.1101/2022.11.09.515637

952 Vega CJ, Peterson DA. 2005. Stem cell proliferative history in tissue revealed by temporal
953 halogenated thymidine analog discrimination. *Nat Methods* **2**:167–169. doi:10.1038/nmeth741

954 Vogg MC, Galliot B, Tsiairis CD. 2019. Model systems for regeneration: Hydra. *Development*
955 **146**. doi:10.1242/dev.177212

956 Weber C. 1981. Structure, histochemistry, ontogenetic development, and regeneration of the
957 ocellus ofCladonema radiatum dujardin (cnidaria, hydrozoa, anthomedusae). *J Morphol*
958 **167**:313–331. doi:10.1002/jmor.1051670306

959 Zhou K, Gu Y, Wang L, Chen J. 2022. Discovery of Cladonema multiramosum sp. nov.
960 (Cnidaria: Hydrozoa: Cladonematidae) using DNA barcoding and life cycle analyses. *Acta*
961 *Oceanol Sin* **41**:44–52. doi:10.1007/s13131-021-1900-5

962

963 **Acknowledgement**

964 We thank R. Deguchi (Miyagi Univ. Education, Japan) for sharing *Cladonema*
965 *pacificum*. We thank D. Umetsu and T. Akiyama for helpful discussion. We thank I.
966 Nagai, A. Sasaki, and H. Nakatani for technical assistance. This work was supported by
967 JSPS/MEXT KAKENHI (grant numbers JP22J01430 to H.N., JP21H05255 to E.K.,
968 JP21H04774, JP21K19206 to M.M., and JP17H06332, JP19K22550, JP22H02762 to

969 Y.N.), JST grant (JPMJCR1852 to E.K. and JPMJSP2114 to S.F.), AMED-Aging
970 (JP21gm5010001 to M.M.), and AMED-PRIME (JP22gm6110025 to Y.N.).
971
972
973 ## Author contributions
974 S.F. conceptualized and designed the project, performed experiments, analyzed data,
975 prepared figures, and wrote the manuscript. E.K. supervised the project. M.M.
976 supervised the project. Y.N. conceptualized, supervised and designed the project,
977 prepared figures, and wrote the manuscript. All authors approved the final manuscript.
978
979
980 ## Competing interests
981 The authors declare no competing interests.
982
983
984 ## Figure legends
985
986 **Figure 1. Regeneration processes and potentials of the *Cladonema* medusa**
987 **tentacle.** (A) The phylogenetic tree of Bilateria and Cnidaria, composed of Anthozoa
988 and Medusozoa. (B) Medusa of *Cladonema pacificum*. U: umbrella, M: manubrium, Ra:
989 radial canal, Ri: ring canal, T: tentacle. (C) Tentacle of *Cladonema* medusa. O: ocellus,
990 TB: tentacle bulb, Br: branch, NC: nematocyte cluster. (D) Tentacle regeneration
991 processes after amputation while retaining the bulb. hpa: hour post-amputation. Yellow
992 arrows indicate nematocyte clusters. n = 234/236 (tentacles). (E) Scheme of the
993 tentacle regeneration that retains the bulb. (F) Distribution of mature nematocytes and
994 localization of muscle fibers during tentacle regeneration. DAPI for poly-γ-glutamate
995 (green) and nuclei (blue), and Phalloidin for F-actin (red). Yellow arrows indicate
996 nematocyte clusters. (G) Neural morphology in the regenerating tentacle stained with
997 the anti-FMRFamide antibody. White arrows indicate neural fibers. (H) The regenerating
998 tentacle is fully functional at 72 hpa. Image of the tentacle capturing prey, brine shrimp
999 (Arrow). (I) The rate of functional tentacles across the regeneration time course. Intact:
1000 n = 40 (tentacles), 0-72 hpa: n = 36. (J) Tentacle regeneration process after removing

1001 the bulb from canals. Dpa: day post-amputation. n = 117/219 (tentacles). Ra: radial
1002 canal, Ri: ring canal. (K) Scheme of tentacle regeneration without bulb. Scale bars: (A-
1003 C, I) 1 mm, (E, F i) 100 μm, (F ii) 50 μm.
1004
1005 **Figure 2. Blastema formation at early phase of tentacle regeneration.**
1006 (A) Distribution of S-phase cells in intact and regenerating tentacle stained with EdU 1 h
1007 pulse labeling. (B) Quantification of EdU^+ cells' distribution in regenerating tentacle. 3
1008 areas defined as basal (grey arrows), middle (pink arrows), distal (red arrows) in (A).
1009 Intact: n = 19 (tentacles), 24 hpa: n = 10, 48 hpa: n = 9, 72 hpa: n = 8. (C) Scheme of
1010 proliferative cells distribution during tentacle regeneration. (D) Distribution of S-phase
1011 and M-phase cells stained with EdU 1 h pulse labeling and anti-Phospho-Histone 3
1012 (PH3) antibody. EdU (green) and PH3 (magenta). Yellow dot squares show each
1013 quantification area (74.72^2 μm^2) in (E, F). (E, F) The proportion of $PH3^+$ and EdU^+ cells
1014 per all cells in each area. Each area: n = 14. (G-I) Distribution of proliferative cells at 24
1015 hpa: (G) After the distal side of tentacle is amputated, (H) after removing the bulb from
1016 canals, and (I) in isolated tentacles at 24 hpa. EdU 1 h pulse labeling. Unpaired two-
1017 tailed *t*-test. $*p < 0.05$, $**p < 0.005$, $***p < 0.001$. Scale bars: (A, G-I) 100 μm, (D) 50 μm.
1018
1019 **Figure 3. Stem cells and progenitor cells in blastema.**
1020 (A) Identification of cell types in blastema stained with anti-β-catenin staining. White
1021 arrow: epithelial cell, white arrow head: i-cell, yellow arrow head: nematocyte. Yellow
1022 dot squares show each quantification area (35.10^2 μm^2) in (B). (B) Cell types in
1023 blastema at 24 hpa by anti-β-catenin staining. n = 3 (areas). (C) FISH images of
1024 *Nanos1* gene expression from the proximal, abaxial side of the tentacle. Distribution of
1025 stem (*Nanos1*$^+$) cells in intact and regenerating tentacle. Yellow arrow indicates main
1026 tentacle, and white arrow indicates new branch. (D) Quantification of *Nanos1*+ cells
1027 distribution in regenerating tentacle. 3 areas defined as basal (grey arrows), middle
1028 (pink arrows), distal (red arrows) in (C). Intact: n = 5, 24 hpa: n = 4 (tentacles), 48 hpa: n
1029 = 4, 72 hpa: n = 5. (E) Images of the intact and regenerating tentacle co-labeled with
1030 *Nanos1* FISH and EdU 1 h pulse labeling. EdU (green) and *Nanos1* (magenta). White
1031 arrowheads indicate EdU^+ and *Nanos1*$^+$ cells. (F) The rate of *Nanos1*+ cells / EdU+
1032 cells in intact and regenerating tentacles. Quantification area of intact tentacle bulb and

1033 blastema is 74.72^2 μm^2. Intact: n = 18, 24 hpa: n = 22. Unpaired two-tailed *t*-test. *p <
1034 0.05, **p < 0.005, ***p < 0.001. Scale bars: (A i, C and E) 50 μm, (A ii) 10 μm.
1035
1036 **Figure 4. Distinct proliferative cell populations during tentacle regeneration.**
1037 (A) Scheme of lineage-tracing experiments using EdU and BrdU. (B) Distribution of
1038 EdU^+ and $BrdU^+$ cells during tentacle regeneration. EdU (green) and BrdU (red). (C)
1039 The number of homeostatic proliferative cells during regeneration. Intact: n = 12
1040 (tentacles), 24 hpa: n = 10, 48 hpa: n = 12, 72 hpa: n = 9. (D) The number of repair-
1041 specific proliferative cells during regeneration. 24 hpa: n = 12, 48 hpa: n = 12, 72 hpa: n
1042 = 6. (E) Scheme of two proliferative cell populations during regeneration. (F) Scheme of
1043 stem cell elimination by 30 Gy X-ray irradiation. Day post-irradiation (dpi). (G)
1044 Distribution of proliferative cells after X-ray irradiation. EdU 1 h pulse labeling. Yellow
1045 dot squares show each quantification area (74.72^2 μm^2) in (H). (H) The rate of EdU^+
1046 cells in blastema. No irradiation: n = 14, X-ray irradiation: n = 7. Unpaired two-tailed *t*-
1047 test. *p < 0.05, **p < 0.005, ***p < 0.001. Scale bars: (B, G) 100 μm.
1048
1049 **Figure 5. Distinct function of two proliferative cell populations.**
1050 (A) Scheme of EdU long-time and BrdU double chasing experiment. (B) The
1051 distributions of EdU^+ and $BrdU^+$ cells during tentacle regeneration. EdU (green) and
1052 BrdU (red). Yellow arrows indicate accumulation of EdU^+ cells at nematocyte clusters in
1053 distal side at 72 hpa. (C) Cell type identification of EdU labeled cells in distal side at 72
1054 hpa by anti-aPKC staining. EdU (green) and aPKC (magenta). Yellow arrow heads
1055 show nematocytes. (D) Cell types of EdU^+ cells on the distal side of a regenerating
1056 tentacle at 72 hpa. Quantification area of regenerating tentacle is 74.72^2 μm^2. n = 10.
1057 (E) Experimental scheme for nematogenesis after 30 Gy X-ray irradiation. (F)
1058 Distribution of mature nematocytes at 72 hpa after irradiation stained with DAPI. DAPI
1059 for poly-γ-glutamate (green) and and nuclei (blue). Yellow arrows indicate nematocyte
1060 clusters. (G) The number of stenoteles (large mature nematocytes) in the regenerating
1061 tentacle at 72 hpa. Ctl: n = 36 (tentacles), X-ray: n = 42. (H) The number of nematocyte
1062 clusters in the regenerating tentacle at 72 hpa. Ctl: n = 36, X-ray: n = 42. (I)
1063 Experimental scheme for tentacle elongation after 30 Gy X-ray irradiation. (J) Length of
1064 regenerating tentacle after irradiation. Ctl: n = 58 (tentacles), 1 dpi: n = 58, 3 dpi: n = 58,

1065 5 dpi: n = 58. (K) Experimental scheme for combining the identification of cell types and
1066 EdU chasing. (L) Identification of cell types of EdU^+ cells in blastema and the distal side
1067 of the regenerating tentacle stained with anti-aPKC staining. EdU (green) and aPKC
1068 (magenta). White arrow: epithelial cell, white arrow head: i-cell, yellow arrow head:
1069 nematocyte. (M) Quantification of cell types in EdU^+ cells at 24 and 72 hpa.
1070 Quantification area of regenerating tentacle is 35.06^2 μm^2. 24 hpa: n = 9, 72 hpa: n =
1071 12. (N) Experimental scheme for measuring of regenerating tentacle after damage to
1072 the blastema from UV exposure. (O) Length of the regenerating tentacle after UV
1073 exposure on blastema. Ctl: n = 12 (tentacles), UV: n = 12. Unpaired two-tailed *t*-test. *p
1074 < 0.05, **$p < 0.005$, ***$p < 0.001$. Scale bars: (B, F) 100 μm, (C, L) 50 μm.
1075
1076 **Figure 6. Summary of *Cladonema* tentacle regeneration and evolutionary history**
1077 **of appendage regeneration.**
1078 (A) When a *Cladonema* medusa tentacle is amputated, wound closure is completed by
1079 24 hpa. After wound healing, repair-specific proliferative cells appear and actively
1080 proliferate at the wound tip. Ectopic cell proliferation on the distal side is gradually
1081 suppressed, and the cell differentiation phase begins. While homeostatic proliferative
1082 cells in the bulb supply nematocytes and epithelial cells, repair-specific proliferative cells
1083 only differentiate into epithelial cells. (B) Blastema formation mechanism during
1084 appendage regeneration across animal evolution. When an appendage is amputated,
1085 repair-specific proliferative cells (stem/progenitor cells) contribute to blastema formation
1086 in both regenerative bilaterians (e.g. salamanders) and cnidarian jellyfish.
1087
1088 **Figure S1. Wound healing, neuron regeneration and the rate of regeneration.**
1089 (A) The process of wound healing from 4 hpa to 24 hpa with Phalloidin and anti-α-
1090 Tubulin antibody. Phalloidin for F-actin (red) and α-Tubulin (green). (B) The extent of
1091 wound healing during tentacle regeneration. 4 hpa: n = 15 (tentacles), 8 hpa: n = 17, 16
1092 hpa: n = 15, 24 hpa: n = 14. (C) Neural morphology in intact tentacle and the
1093 regenerating tentacle stained with the anti-FMRFamide antibody. Yellow allows indicate
1094 cell bodies of FMRFamide neurons. FMRFamide (magenta). (i, ii) Intact whole tentacle,
1095 (iii, iv) basal side of intact tentacle, (v, vi) regenerating tentacle at 24 hpa. (D) Neural
1096 morphology in the regenerating tentacle stained with the anti-acetylated-Tubulin

antibody. White arrows indicate neural fibers. acetylated-Tubulin (green). (E) The rate of the tentacle regeneration after removing the bulb from canals. (F) Images of the isolated tentacle without bulb at 1 dpa and 7 dpa. (G) Images of the isolated whole tentacle 1 dpa and 7 dpa. Scale bars: (A, C i-iii, v and D i, iii) 100 μm, (C iv, vi and D ii, iv) 50 μm, (F, G) 1 mm.

Figure S2. The distribution of mitotic cells during regeneration.
(A) Distribution of mitotic cells detected by anti-PH3 in regenerating tentacle. (B) Quantification of $PH3^+$ cells distribution in regenerating tentacle. Intact: n = 11 (tentacles), 24 hpa: n = 10, 48 hpa: n = 9, 72 hpa: n = 8.

Figure S3. The distribution of stem cells in intact tentacle and regenerating tentacle.
(A) Expression pattern of *Nanos1* in intact tentacle by FISH. (B) Expression pattern of *Piwi* in intact tentacle by FISH. (C) Distribution of stem (*Piwi*$^+$) cells in intact and regenerating tentacle. White arrowhead indicates *Piwi*$^+$ cells. (D) Images of the proximal abaxial side of regenerating tentacle co-labeled with *Piwi* expression and EdU. EdU 1 h pulse labeling. White arrowhead indicates *Piwi*$^+$ and EdU^+ cells. (E) The rate of *Piwi*$^+$ cells / EdU^+ cells around blastema in regenerating tentacles. n = 5 (tentacles). Scale bars: (A and B) 100 μm, (C and D) 50 μm.

Figure S4. Distribution and increase of homeostatic proliferative cells during tentacle regeneration.
(A) Transition of labeled cells during regeneration by chasing EdU signals. EdU 1 h pulse labeling before amputation. (B) Experiment scheme of chasing the cells in bulb labeled by DiI. (C) No migration of DiI labeled cells in bulb from amputation to 24 hpa. EdU 1h pulse labeling at 24 hpa. (D) The comparison of proliferative cell number in intact vs no amputation vs 24 hpa. EdU 1 h pulse labeling before amputation. (E) Quantification of cells labeled before amputation. Intact: n = 6 (tentacles), 24 h: n = 6, 24 hpa: n = 6. Unpaired two-tailed *t*-test. $^*p < 0.05$, $^{**}p < 0.005$, $^{***}p < 0.001$. Scale bars: (A, C and D) 100 μm.

1129 **Figure S5. *Nanos1*$^{+}$ cells in bulb decreased after X-ray irradiation.**
1130 (A) Relative expression of *Nanos1* after irradiation by qPCR. (B) Expression of *Nanos1*
1131 in bulb of intact tentacle after irradiation by FISH. (C) Quantification of *Nanos1*$^{+}$ cells
1132 number in bulb. Control: n = 6 (tentacles), 3 dpi: n = 6. Unpaired two-tailed *t*-test. *p <
1133 0.05, **p < 0.005, ***p < 0.001. Scale bars: (B) 100 μm.
1134
1135 **Figure S6. EdU long incorporation also labeled nematocyte progenitors.**
1136 (A) Nematocyte progenitor cells in bulb of intact tentacle with dual staining of *Nowa*
1137 FISH and EdU staining. EdU 1 h or 24 h pulse labeling. (B) The rate of *Nowa*$^{+}$ cells /
1138 EdU^{+} cells in intact tentacle. 1 h: n = 20 (tentacles), 24 h: n = 22. (C) Nematocyte
1139 progenitor cells in bulb with dual staining of *Mcol1* FISH and EdU staining. EdU 1 h or
1140 24 h pulse labeling. Unpaired two-tailed *t*-test. *p < 0.05, **p < 0.005, ***p < 0.001.
1141 Scale bars: (A, C) 50 μm.
1142
1143 **Figure S7. Similar pattern between β-catenin and aPKC antibody staining**
1144 Identification of cell types in blastema stained by β-catenin and aPKC antibody staining.
1145 Scale bar: 50 μm.
1146
1147 **Figure S8. Injury-responsive cells decreased after UV exposure on blastema.**
1148 (A) Experimental scheme depicting the combination of EdU chasing and UV exposure.
1149 EdU 1 h pulse labeling at 24 hpa. (B) Bleaching of Hoechst signal only in UV exposure
1150 area at 24 hpa. White dot square is UV exposure area. (C) Distribution of EdU labeled
1151 cells 1 day after UV exposure. (D) The number of EdU^{+} cells in UV exposed tentacle at
1152 48 hpa. Ctl: n = 7 (tentacles), UV: n = 8. Unpaired two-tailed *t*-test. *p < 0.05, **p <
1153 0.005, ***p < 0.001. Scale bars: (B, C) 100 μm.
1154

Figure 1

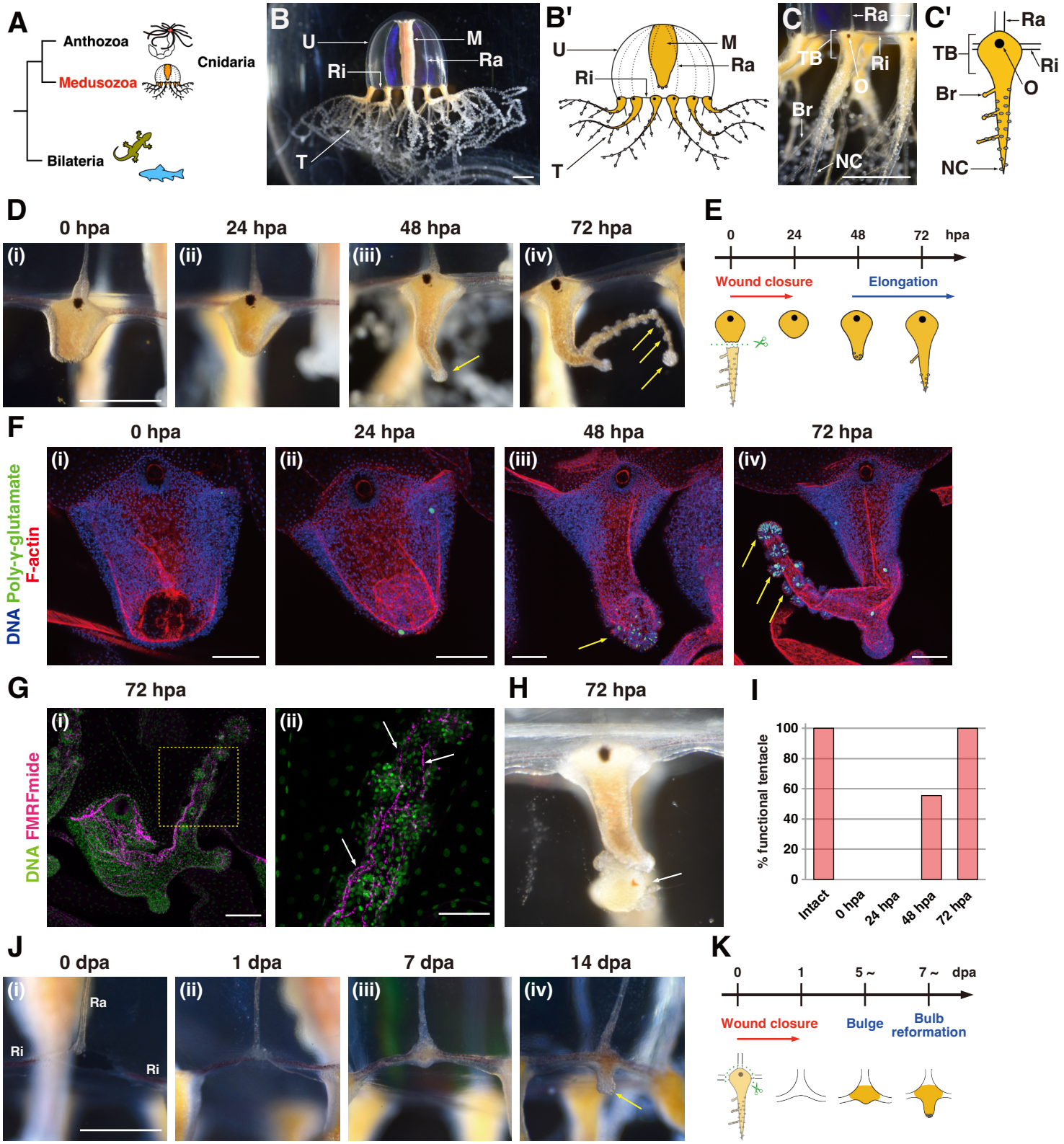
A
Anthozoa
Medusozoa
Cnidaria
Bilateria
B
U
M
Ra
Ri
T
B'
U
M
Ra
Ri
T
C
Ra
TB
Ri
O
Br
NC
C'
Ra
TB
Ri
O
Br
NC
D
0 hpa
24 hpa
48 hpa
72 hpa
(i)
(ii)
(iii)
(iv)
E
0
24
48
72
hpa
Wound closure
Elongation
F
0 hpa
24 hpa
48 hpa
72 hpa
DNA Poly-γ-glutamate
F-actin
(i)
(ii)
(iii)
(iv)
G
72 hpa
DNA FMRFmide
(i)
(ii)
H
72 hpa
I
% functional tentacle
100
80
60
40
20
0
Intact
0 hpa
24 hpa
48 hpa
72 hpa
J
0 dpa
1 dpa
7 dpa
14 dpa
(i)
(ii)
(iii)
(iv)
Ra
Ri
Ri
K
0
1
5 ~
7 ~
dpa
Wound closure
Bulge
Bulb reformation

Figure 2

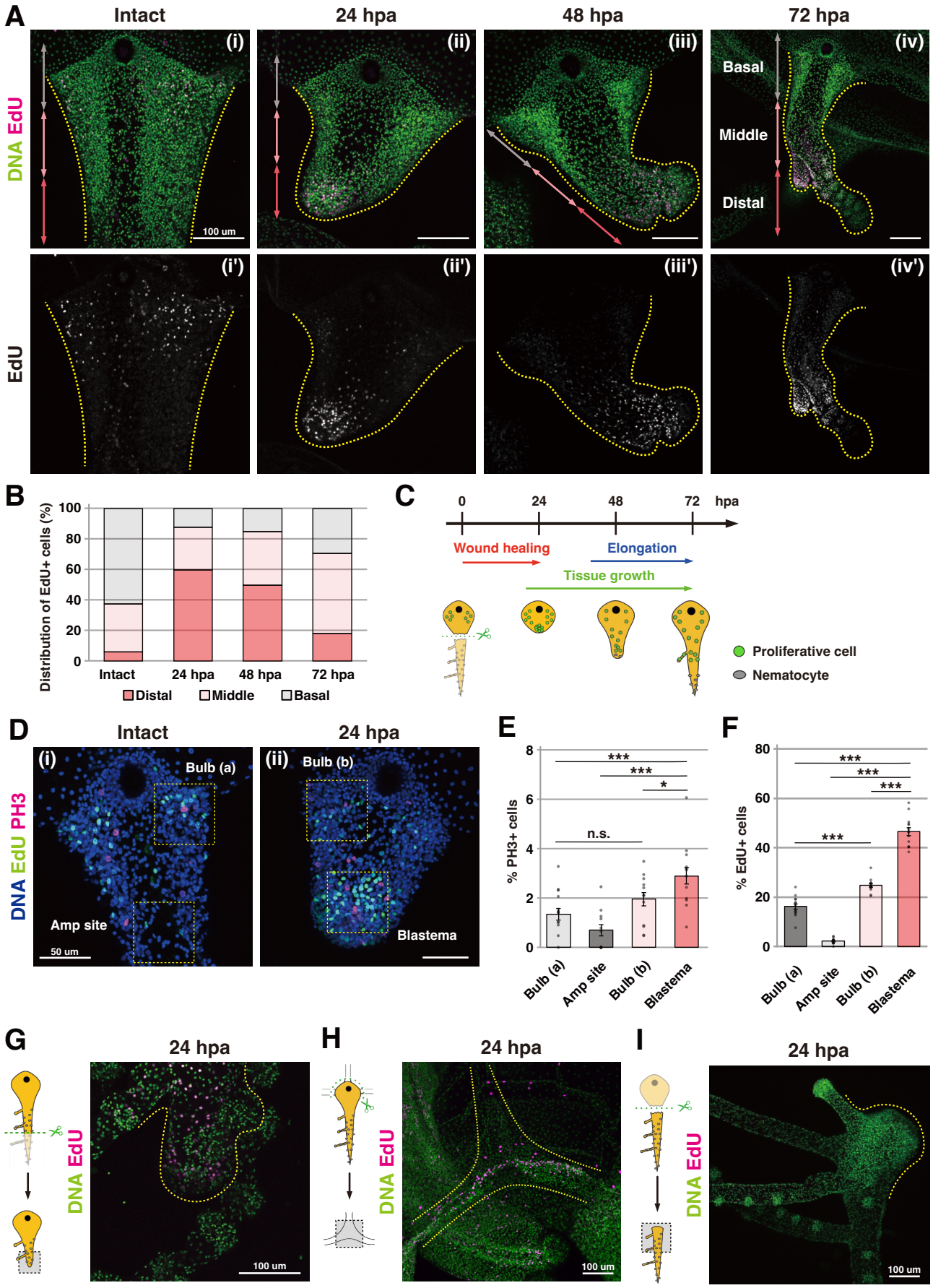
A
Intact
24 hpa
48 hpa
72 hpa
DNA EdU
(i)
(ii)
(iii)
(iv)
Basal
Middle
Distal
100 um
EdU
(i')
(ii')
(iii')
(iv')
B
Distribution of EdU+ cells (%)
100
80
60
40
20
0
Intact
24 hpa
48 hpa
72 hpa
Distal
Middle
Basal
C
0
24
48
72
hpa
Wound healing
Elongation
Tissue growth
Proliferative cell
Nematocyte
D
Intact
24 hpa
DNA EdU PH3
(i)
Bulb (a)
Amp site
50 um
(ii)
Bulb (b)
Blastema
E
% PH3+ cells
8
6
4
2
0
***
***
*
n.s.
Bulb (a)
Amp site
Bulb (b)
Blastema
F
% EdU+ cells
80
60
40
20
0
***
***
***
***
Bulb (a)
Amp site
Bulb (b)
Blastema
G
24 hpa
DNA EdU
100 um
H
24 hpa
DNA EdU
100 um
I
24 hpa
DNA EdU
100 um

Figure 3

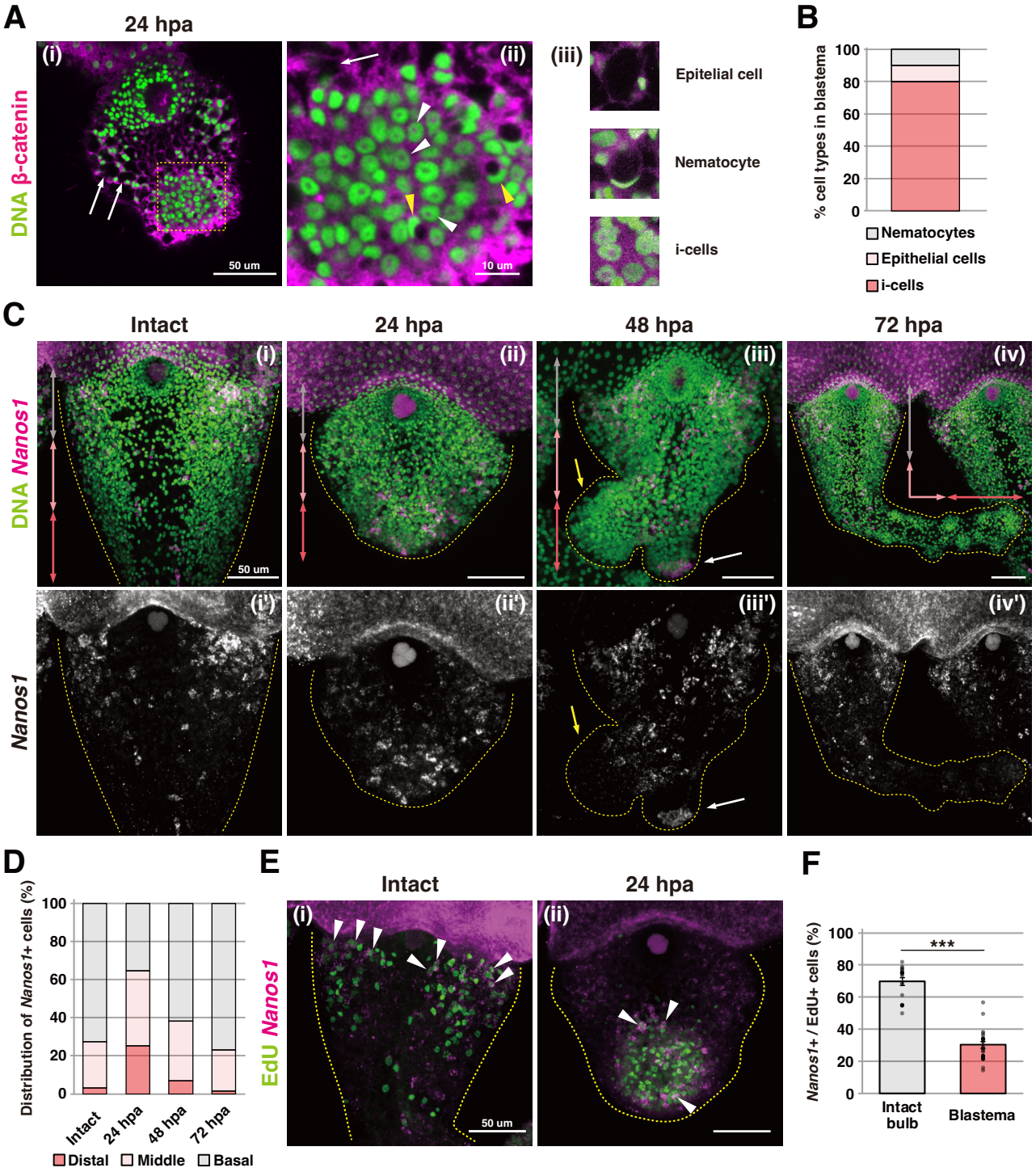
A
24 hpa
DNA β-catenin
(i)
(ii)
(iii)
50 um
10 um
Epitelial cell
Nematocyte
i-cells
B
% cell types in blastema
100
80
60
40
20
0
Nematocytes
Epithelial cells
i-cells
C
Intact
24 hpa
48 hpa
72 hpa
DNA Nanos1
Nanos1
(i)
(ii)
(iii)
(iv)
(i')
(ii')
(iii')
(iv')
50 um
D
Distribution of Nanos1+ cells (%)
Intact
24 hpa
48 hpa
72 hpa
Distal
Middle
Basal
E
Intact
24 hpa
EdU Nanos1
(i)
(ii)
50 um
F
Nanos1+ / EdU+ cells (%)
***
Intact bulb
Blastema

Figure 4

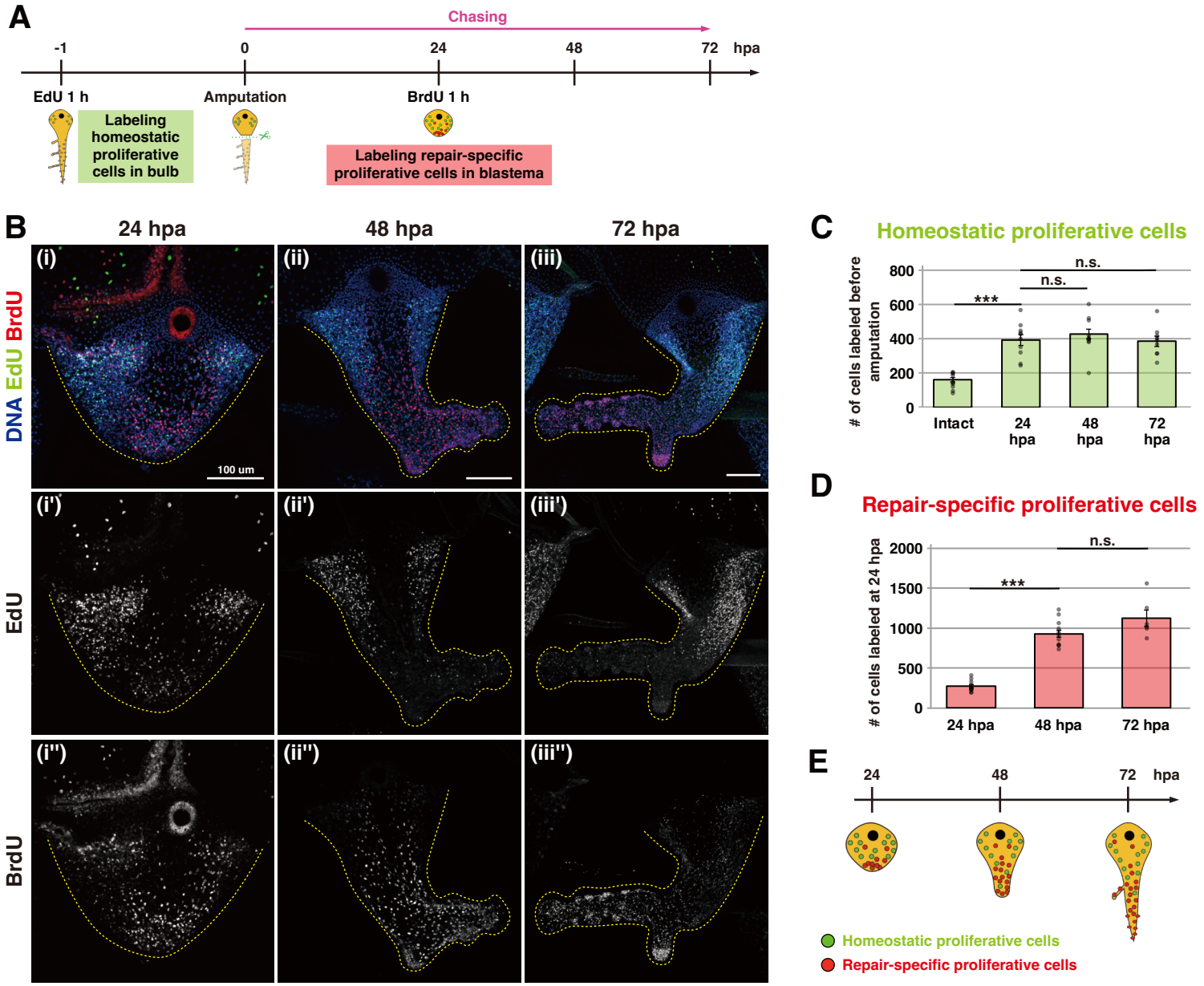
A
Chasing
-1
0
24
48
72
hpa
EdU 1 h
Amputation
BrdU 1 h
Labeling homeostatic proliferative cells in bulb
Labeling repair-specific proliferative cells in blastema
B
24 hpa
48 hpa
72 hpa
DNA EdU BrdU
EdU
BrdU
(i)
(ii)
(iii)
(i')
(ii')
(iii')
(i'')
(ii'')
(iii'')
100 um
C
Homeostatic proliferative cells
# of cells labeled before amputation
800
600
400
200
0
***
n.s.
n.s.
Intact
24 hpa
48 hpa
72 hpa
D
Repair-specific proliferative cells
# of cells labeled at 24 hpa
2000
1500
1000
500
0
***
n.s.
24 hpa
48 hpa
72 hpa
E
24
48
72
hpa
Homeostatic proliferative cells
Repair-specific proliferative cells

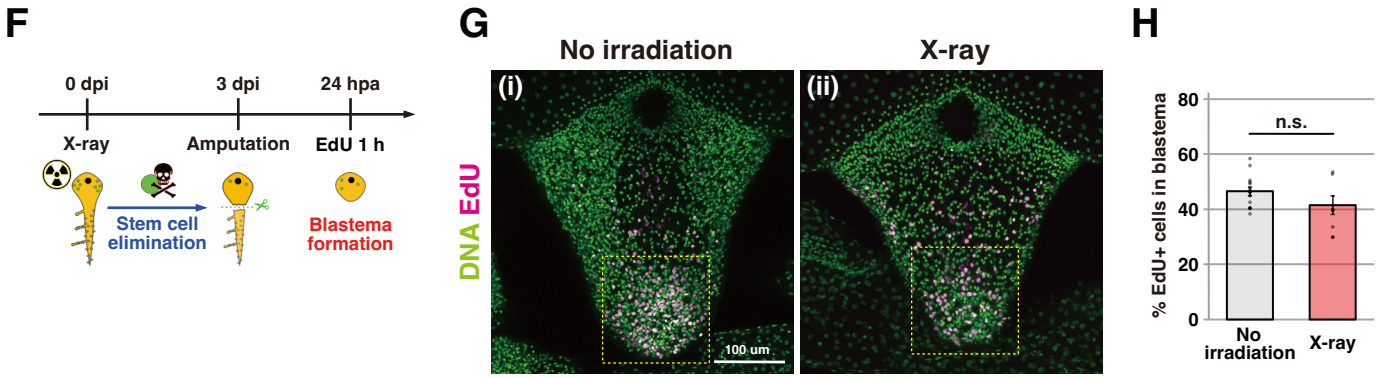
F
0 dpi
3 dpi
24 hpa
X-ray
Amputation
EdU 1 h
Stem cell elimination
Blastema formation
G
No irradiation
X-ray
DNA EdU
(i)
(ii)
100 um
H
% EdU+ cells in blastema
80
60
40
20
0
n.s.
No irradiation
X-ray

Figure 5

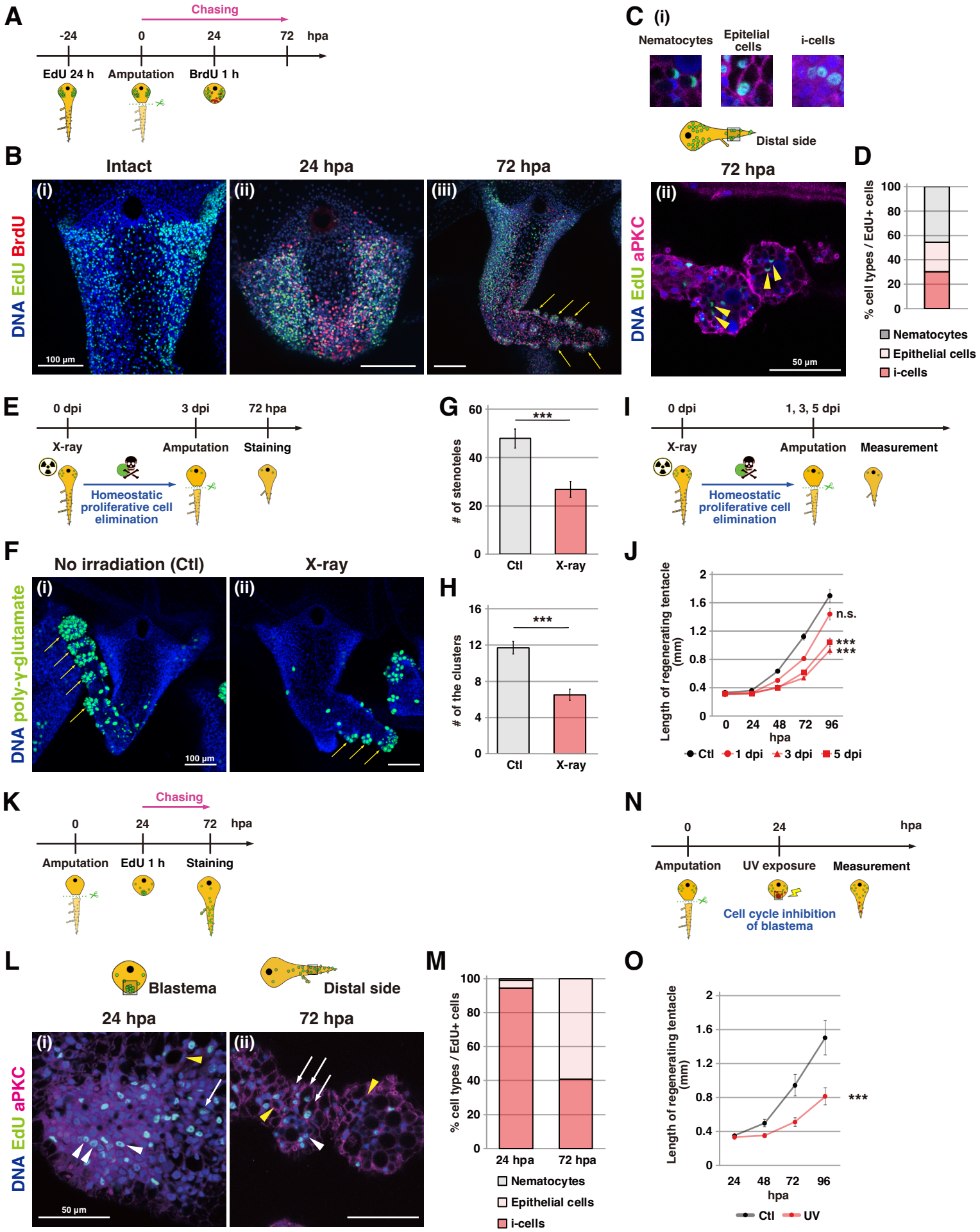
A
Chasing
-24
0
24
72
hpa
EdU 24 h
Amputation
BrdU 1 h
B
Intact
24 hpa
72 hpa
DNA EdU BrdU
(i)
(ii)
(iii)
100 µm
C (i)
Nematocytes
Epitelial cells
i-cells
Distal side
72 hpa
DNA EdU aPKC
50 µm
D
% cell types / EdU+ cells
Nematocytes
Epithelial cells
i-cells
E
0 dpi
3 dpi
72 hpa
X-ray
Amputation
Staining
Homeostatic proliferative cell elimination
G
# of stenoteles
***
Ctl
X-ray
I
0 dpi
1, 3, 5 dpi
X-ray
Amputation
Measurement
Homeostatic proliferative cell elimination
F
No irradiation (Ctl)
X-ray
DNA poly-γ-glutamate
H
of the clusters
J
Length of regenerating tentacle (mm)
n.s.
hpa
Ctl
1 dpi
3 dpi
5 dpi
K
Chasing
0
24
72
hpa
Amputation
EdU 1 h
Staining
N
0
24
hpa
Amputation
UV exposure
Measurement
Cell cycle inhibition of blastema
L
Blastema
Distal side
24 hpa
72 hpa
DNA EdU aPKC
50 µm
M
% cell types / EdU+ cells
24 hpa
72 hpa
Nematocytes
Epithelial cells
i-cells
O
Length of regenerating tentacle (mm)
hpa
Ctl
UV

Figure 6

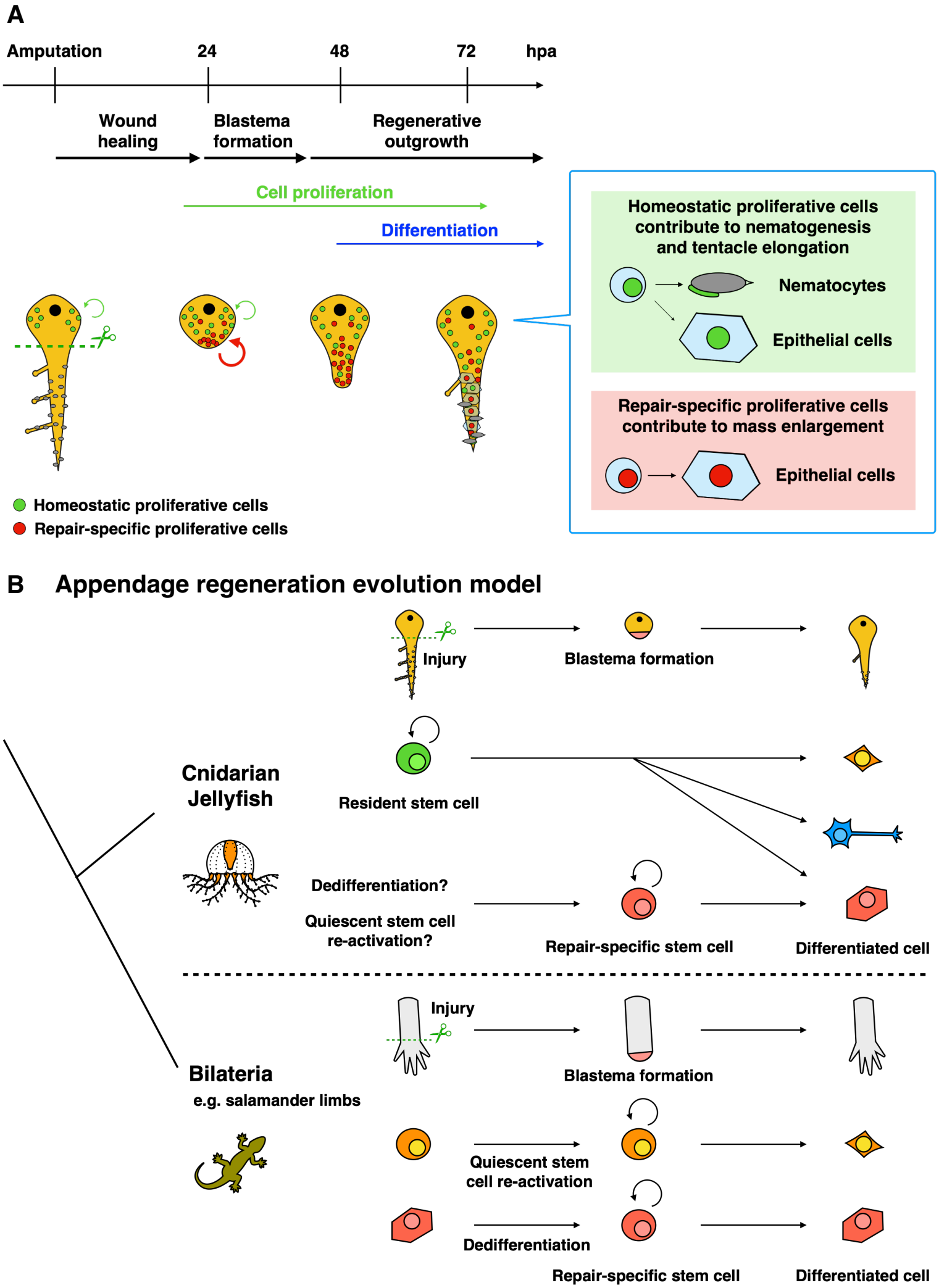
A
Amputation
24
48
72
hpa
Wound healing
Blastema formation
Regenerative outgrowth
Cell proliferation
Differentiation
Homeostatic proliferative cells contribute to nematogenesis and tentacle elongation
Nematocytes
Epithelial cells
Repair-specific proliferative cells contribute to mass enlargement
Epithelial cells
Homeostatic proliferative cells
Repair-specific proliferative cells
B Appendage regeneration evolution model
Injury
Blastema formation
Cnidarian Jellyfish
Resident stem cell
Dedifferentiation?
Quiescent stem cell re-activation?
Repair-specific stem cell
Differentiated cell
Injury
Bilateria
e.g. salamander limbs
Blastema formation
Quiescent stem cell re-activation
Dedifferentiation
Repair-specific stem cell
Differentiated cell